



NKS-338
ISBN 978-87-7893-420-8

CFD and FEM modeling of blowdown of gas into pressure suppression pool

Timo Pättikangas
Antti Timperi
Qais Saifi

VTT Technical Research Centre of Finland

May 2015

Abstract

Computational Fluid Dynamics (CFD) and Finite Element Methods (FEM) used for modelling pressure suppression pool during a postulated Large-Break Loss-Of-Coolant-Accident (LB-LOCA) are summarized. The CFD methods used for the simulation of the early stage of the LB-LOCA are applied to a sector model of a BWR. Fluid-Structure Interaction (FSI) calculations are performed for the PPOOLEX test facility and a sector model of BWR. Acoustic FEM method is applied to a model of BWR containment.

FSI calculations using explicit and implicit two-way coupling of Star-CCM+ and Abaqus codes are performed. The implicit simulations enabled the use of fairly large time steps, even when the ratio of structure density to fluid density was decreased such that the explicit solution became severely unstable. Simulations of the early non-condensable phase for a realistic BWR containment showed stable calculations also with explicit coupling when compressible water was assumed.

Simulations of a boiling water reactor (BWR) containment with an acoustic FSI FEM model were performed. The BWR containment with 16 vent pipes was loaded stochastically through the pipes. Different statistical cases were considered for applying the loads. A normal distribution curve with the mean value and standard deviation was developed for each varied parameter. The results from different statistical cases were compared.

The CFD model for Large Interfaces in two-phase calculations is reviewed and the use of the model for large gas bubbles in pressure suppression pool is discussed. The early stage of LB-LOCA is calculated with a 90° sector model of BWR containment.

Key words

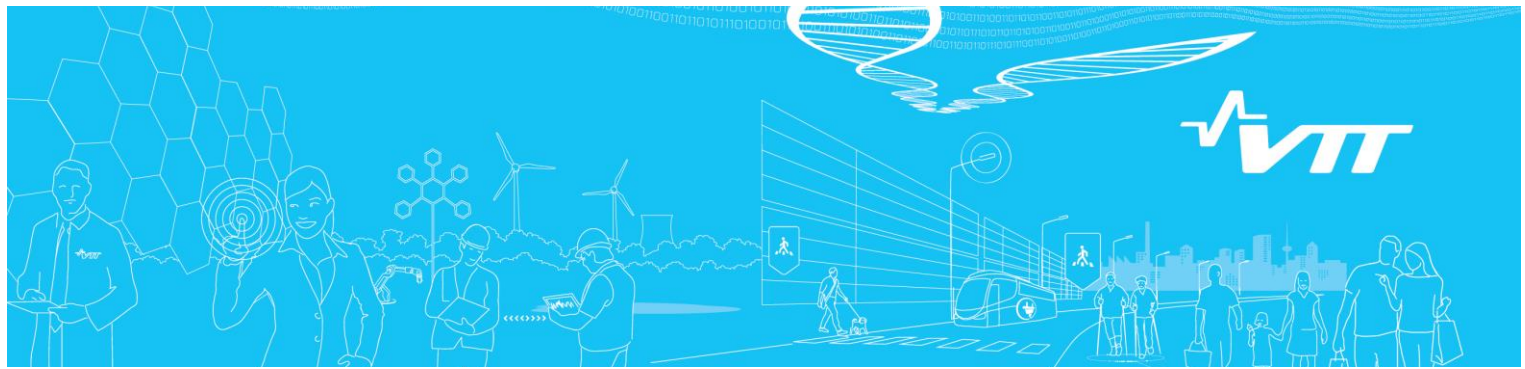
Condensation pool, pressure suppression pool, BWR, CFD, fluid-structure interaction, FSI, chugging, LOCA

Acknowledgment

NKS conveys its gratitude to all organisations and persons who by means of financial support or contributions in kind have made the work presented in this report possible.

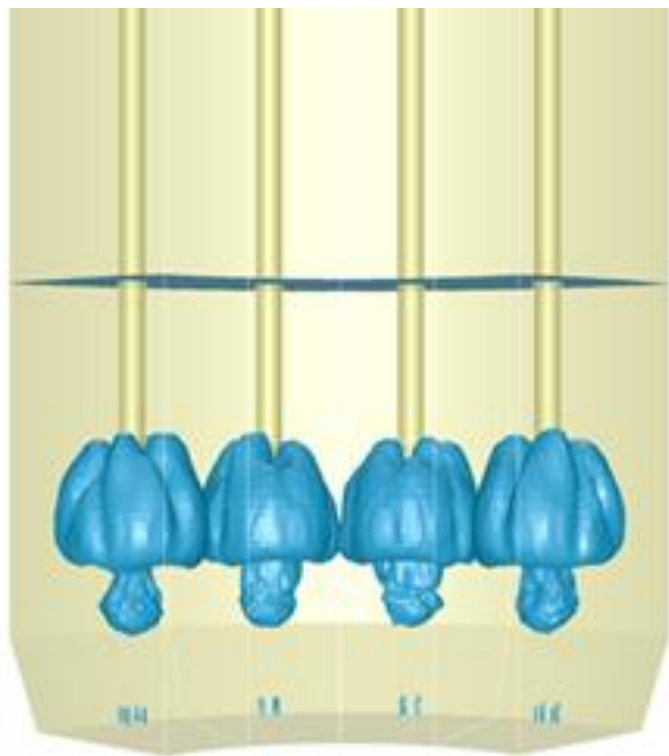
Disclaimer

The views expressed in this document remain the responsibility of the author(s) and do not necessarily reflect those of NKS. In particular, neither NKS nor any other organization or body supporting NKS activities can be held responsible for the material presented in this report.



RESEARCH REPORT



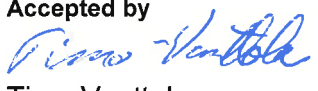
VTT-R-00868-15



CFD and FEM modeling of blowdown of gas into pressure suppression pool

Authors: Timo Pättikangas, Antti Timperi and Qais Saifi

Confidentiality: Public

Report's title		
CFD and FEM modelling of blowdown of gas into pressure suppression pool		
Customer, contact person, address		Order reference
1. Valtion ydinjätehuoltorahasto, Työ- ja elinkeinoministeriö, PL 32, 00023 VALTIONEUVOSTO 2. Karin Andgren, Nordic nuclear safety research (NKS), Programme Manager NKS-R, VATTENFALL, SE-169 92 Stockholm, SWEDEN		1. SAFIR2014 Programme: Dnro SAFIR 17/2014 2. NKS Contract no. AFT/NKS-R(14)90/7
Project name		Project number/Short name
Numerical modelling of condensation pool		85490 / NUMPOOL 2014
Author(s)		Pages
Timo Pättikangas, Antti Timperi and Qais Saifi		46
Keywords		Report identification code
Condensation pool, pressure suppression pool, BWR, CFD, fluid-structure interaction, FSI, chugging, LOCA		VTT-R-00868-15
Summary		
<p>The Computational Fluid Dynamics (CFD) and Finite Element Methods (FEM) used for modelling pressure suppression pool during a postulated Large-Break Loss-Of-Coolant-Accident (LB-LOCA) are summarized. The CFD methods used for the simulation of the early stage of the LB-LOCA are described and applied to a sector model of a BWR. Fluid-Structure Interaction (FSI) calculations are performed for the PPOOLEX test facility and a sector model of a BWR. Acoustic FEM method is applied to a model of BWR containment.</p> <p>FSI calculations using explicit and implicit two-way coupling of Star-CCM+ and Abaqus codes are performed. The implicit simulations enabled the use of fairly large time steps, even when the ratio of structure density to fluid density was decreased such that the explicit solution became severely unstable. Simulations of the early non-condensable phase for a realistic BWR containment showed stable calculations also with explicit coupling when compressible water was assumed.</p> <p>Simulations of a boiling water reactor (BWR) containment with an acoustic FSI FEM model were performed. The BWR containment with 16 vent pipes was loaded stochastically through the pipes. Different statistical cases were considered for applying the loads. A normal distribution curve with the mean value and standard deviation was developed for each varied parameter. The results from different statistical cases were compared.</p> <p>The CFD model for Large Interfaces in two-phase calculations is reviewed and the use of the model for large gas bubbles in pressure suppression pool is discussed. The early stage of LB-LOCA is calculated with a 90° sector model of BWR containment.</p>		
Confidentiality	Public	
Espoo 15.4.2015		
Written by	Reviewed by	Accepted by
		
Timo Pättikangas Principal Scientist	Mikko Manninen Principal Scientist	Timo Vanttola Head of Research Area
VTT's contact address		
VTT Technical Research Centre of Finland Ltd, P.O.B. 1000, FI-02044 VTT, Finland		
Distribution (customer and VTT)		
Karin Andgren (NKS), STUK, Vesa Suolanen (VTT), Pavel Kudinov (KTH), Vesa Tanskanen (LUT), Markku Puustinen (LUT), Heikki Purhonen (LUT), Jani Laine (LUT), SAFIR2014 Reference Group 4		
<p><i>The use of the name of VTT Technical Research Centre of Finland Ltd in advertising or publishing of a part of this report is only permissible with written authorisation from VTT Technical Research Centre of Finland Ltd.</i></p>		

Preface

This work has been carried out in the NUMPOOL project of the SAFIR2014 programme (The Finnish Research Programme on Nuclear Power Plant Safety). The project has been funded by Valtion ydinjätehuoltorahasto, VTT and NKS (Nordic nuclear safety research). The authors are grateful for comments obtained from the members of the SAFIR2010 Reference Group 4 and from the Northnet Roadmap 3 Reference Group.

Espoo, 25 March 2015

Authors

Contents

Preface.....	3
Contents.....	4
1. Introduction.....	5
2. Fluid-structure interaction calculations	6
2.1 Propagation of a pressure pulse	6
2.2 Piston FSI problem	8
2.3 Modelling of the PPOOLEX facility.....	11
2.4 Modelling of a BWR containment.....	16
3. Simulation of BWR containment with acoustic FSI model	22
3.1 FEM model of the BWR containment.....	22
3.2 Stochastic load amplitude (Case 1)	23
3.3 Stochastic load period (Case 2)	24
3.4 Combination of all three statistics (Case 3)	26
3.5 Comparisons of the results from all three cases	28
4. CFD calculations of blowdown in a BWR containment.....	32
4.1 Large Interface model.....	32
4.2 CFD model for a sector of a BWR containment	33
4.3 CFD calculation of the early phase of Large-Break LOCA	33
5. Summary and conclusions	43
References.....	45

1. Introduction

In boiling water reactors (BWRs), the major function of the containment system is to protect the environment if a loss-of-coolant accident (LOCA) should occur. The containment is designed to accommodate the loads generated in hypothetical accidents, such as sudden rupture of a main steam line. In such an accident, a large amount of steam is suddenly released in the containment. An essential part of the pressure suppression containment is a water pool, where condensation of released steam occurs.

In a BWR, the pressure suppression containment typically consists of a drywell and a wetwell with a water pool. In the hypothetical LOCA, steam and air flow from the drywell through vent pipes to the wetwell, where the outlets of the vent pipes are submerged in the water pool. In the early part of the accident, mainly non-condensable air or nitrogen flows through the vent pipes into the wetwell. Then, the volume fraction of vapor increases in the gas mixture. When all the non-condensable gas from the drywell has been blown into the wetwell, the blowdown consists of pure vapor. At this stage, so-called chugging effect may occur, which means periodic formation and rapid condensation of large vapor bubbles at the vent outlets (Lahey and Moody, 1993). The rapid condensation of the vapor bubbles may induce significant pressure loads on the structures in the pressure suppression pool and on the containment.

Determination of the chugging pressure source from the PPOOLEX experiments is studied with the acoustic-structural Fluid-Structure Interaction (FSI) model. The time signal for the pressure source is taken from pressure signal measured near the vent pipe exit for a rapidly collapsing steam bubble. The linearity of the FSI model enables linear scaling of the load magnitude and the pool response. Hence the pressure source magnitude is scaled according to measured pool pressures and displacements. Different water sonic velocities and ways for applying the pressure source at the vent exit as well as the effect of the containment gas volumes are studied in the modelling.

Earlier FSI simulations of the POOLEX and PPOOLEX facilities have been numerically unstable with explicit two-way coupling (Timperi et al., 2006; Pättikangas et al., 2008). External middleware for transferring the boundary data between the CFD and FEM models was used in the earlier work. In the explicit coupling, the loads and displacements between the CFD and FEM models are exchanged only once per time step, i.e. without iteration of the coupled FSI solution inside time step. The numerical instability can be usually prevented with implicit coupling, where iteration inside time step is performed by exchanging the boundary data several times during one time step (see e.g. Causin et al., 2004; Sigrist and Abouri, 2006). The Star-CCM+ CFD and the Abaqus FEM codes can be coupled without external software, and also the implicit method is available. Therefore, these codes are studied in this work in order to achieve numerically stable, fully coupled FSI simulations of the condensation pools. The performance of Star-CCM+ for modelling a propagating pressure wave in water is first studied. The explicit and implicit coupling methods are then tested with a simplified FSI problem and the results are compared with an acoustic-structural Abaqus FSI simulation. Finally, implicit FSI simulations of the PPOOLEX and BWR containment pools are performed.

The acoustic FSI model developed in the previous works (Timperi et al., 2014; Timperi et al., 2013) is developed further for stochastic simulations of the BWR containment. In the previous work, for different load shapes determined from the full-scale JAERI experiments (Kukita and Namatame, 1985), the stochastic simulations for desynchronized chug events were studied. Results for different load shapes and two water sonic velocities were presented and compared. In this study, a single load shape from previous work (Timperi et al., 2014) is considered. Combination of different statistics, such as load desynchronization, load amplitude variation and load period variation are simulated. For the chug events desynchronization, standard deviation value and mean value from the previous study have

been used, whereas for load amplitude and load period new mean values and standard deviations are applied based on the data of Kukita and Namatame (1985). Two simulations for each statistic are performed, respectively with water sonic velocities of 450 and 1412 m/s.

This report summarizes three different approaches for the analysis of pressure loads in the containment of BWR during large-break LOCA. In Section 2, FSI calculations with coupled CFD and FEM codes are described. The methods are applied to a sector model of BWR containment. In Section 3, acoustic FEM calculations are described, where the effect of the stochastic behavior of the vent pipes during steam condensation is studied. In Section 4, CFD methods for the analysis of large-break LOCA are described and applied to 90° sector model of BWR containment. Finally, Section 5 summarizes the work.

2. Fluid-structure interaction calculations

2.1 Propagation of a pressure pulse

The one-dimensional problem of propagation of a sinusoidal pressure pulse was first solved with Star-CCM+ by using different time steps and time discretizations. The problem is the same that was used earlier for studying the accuracies of the Star-CD and Abaqus codes for the acoustic calculation (Pättikangas et al., 2011). For the fluid, density $\rho_0 = 1000 \text{ kg/m}^3$ and speed of sound $c = 1000 \text{ m/s}$ were assumed, which correspond approximately to the values of water. The compressible liquid was modelled in Star-CCM+ by a user defined equation of state. A constant speed of sound was specified and the water density and density pressure derivative were specified by field functions as

$$\rho = \rho_0 + (p - p_0) / c^2 \quad (1)$$

$$\frac{d\rho}{dp} = \frac{1}{c^2} \quad (2)$$

where the reference pressure is $p_0 = 1 \text{ bar}$. Pressure boundary condition at the model boundary was

$$p = \begin{cases} \frac{\hat{p}}{2} \left(1 - \cos \frac{2\pi t}{\tau} \right), & 0 \leq t < \tau \\ 0, & t \geq \tau \end{cases} \quad (3)$$

where τ is the duration of the pulse defined by the speed of sound and the pulse wavelength: $\tau = \lambda/c$. The wavelength was chosen as $\lambda = 1 \text{ m}$ so that the duration becomes $\tau = 1 \text{ ms}$. Amplitude of the pulse was chosen $\hat{p} = 1 \text{ bar}$, so that only small density variations result.

Cell length was chosen as $\Delta x = 0.025 \text{ m}$ based on the earlier study. The SIMPLE pressure-correction method was used for the flow solution. Time discretization was performed either with the first order accurate two time-level method or the second order accurate three time-level method. Either single- or double-precision machine accuracy was used in the calculations. The calculation parameters are listed in Table 1. The Courant number based on sound speed is $CFL_c = c\Delta t/\Delta x$; it represents length which the sound wave travels during one time step relative to the cell length. In the following results, calculation error is defined as the numerical damping of the peak pressure when it has arrived at monitoring location:

$$\varepsilon = \frac{\hat{p} - \hat{p}_{calc}}{\hat{p}} \quad (4)$$

Table 1. Calculation parameters for solving the pressure pulse.

Δx [m]	$\lambda/\Delta x$	Δt [μs]	$\tau/\Delta t$	$CFL_c = c\Delta t/\Delta x$
0.025	40	0.5 ... 5	200 ... 2000	0.02 ... 0.2

Figure 1 shows the pressure pulse after 10 meters of propagation for the first order time discretization using single- and double-precision solution. The corresponding error behaviors are plotted in Fig. 2. It is seen that the numerical damping of the pressure pulse is considerable with first order time discretization unless a very short time step is used. The single- and double-precision solutions yield same results for large time steps while double-precision is required for small time steps. The convergence rate is approximately first order for small time steps and double-precision solution.

Figure 3 shows the pressure pulse after 2.5 and 10 meters of propagation for the first and second order time discretizations using time step of 2 μs . It is seen that the second order time discretization preserves the pulse amplitude well, but results in oscillatory solution and slight over-prediction of the peak pressure.

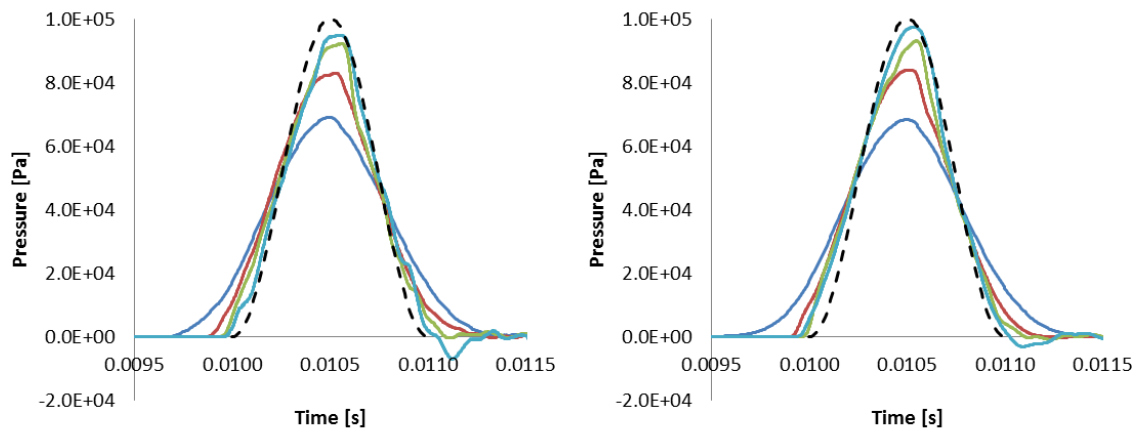


Figure 1. Pressure pulse at $x = 10$ m for first order time discretization using single-precision (left) and double-precision (right) solutions. (— $\Delta t = 5 \mu s$, — $\Delta t = 2 \mu s$, — $\Delta t = 1 \mu s$, — $\Delta t = 0.5 \mu s$, -- Exact)

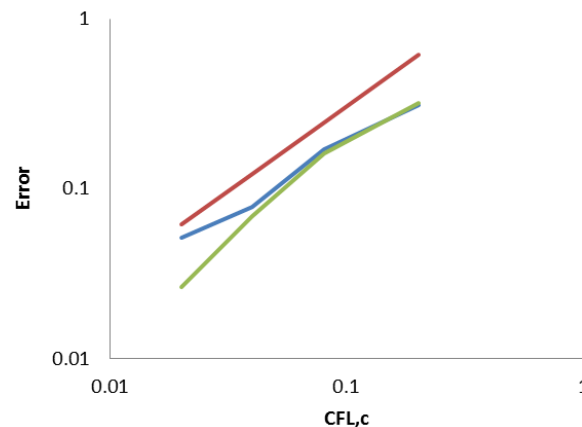


Figure 2. Reduction pressure pulse amplitude error at $x = 10$ m for first order time discretization. (— Single-precision, — Double precision, — 1. order slope)

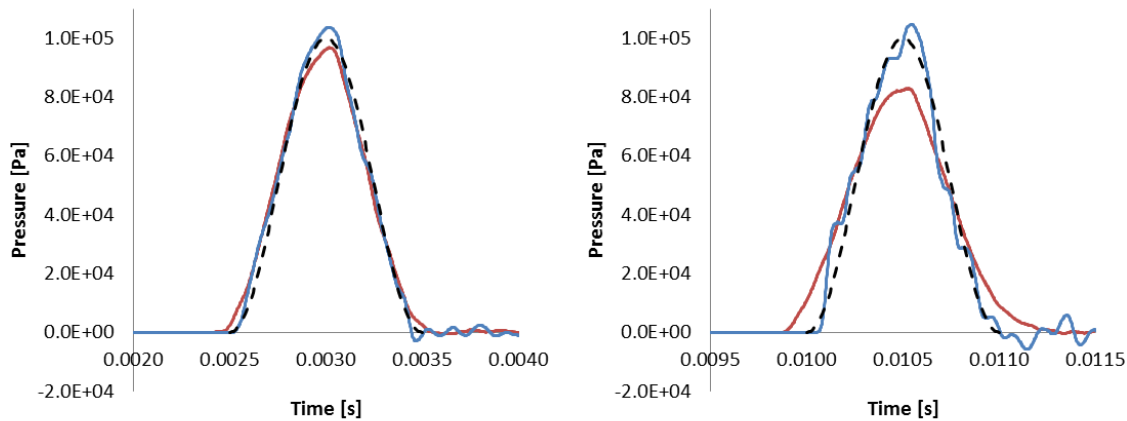


Figure 3. Pressure pulse at $x = 2.5$ m (left) and $x = 10$ m (right) for first and second order time discretization using single-precision solution. (— 1. order, — 2. order, -- Exact)

2.2 Piston FSI problem

The one-dimensional piston problem, shown schematically in Fig. 4, was used for testing the coupled FSI calculations in a simple case. The problem is essentially same that was used earlier for studying coupling between Star-CD and Abaqus by using the MpCCI middleware (Pättikangas et al., 2011). The length of the cylinder was $L = 1$ m with a cross-sectional area $A = 0.01$ m². Density $\rho_0 = 1000$ kg/m³ and speed of sound $c = 1000$ m/s were used for the fluid. The piston mass was chosen 0.1 or 0.01 times the fluid mass, i.e. $m_s = 1$ or 0.1 kg, and the spring stiffness was $k = 40$ or 4 MN/m. The natural frequency of the pistons without fluid would be then

$$f_s = \frac{1}{2\pi} \sqrt{\frac{k}{m_s}} \approx 1010 \text{ Hz} \quad (5)$$

The natural frequencies of the systems with incompressible fluid would be

$$f_{s+f} = \frac{1}{2\pi} \sqrt{\frac{k}{m_s + m_f}} \approx 303 \text{ or } 100 \text{ Hz} \quad (6)$$

The piston had initially small unbalanced force and was left free to oscillate. The force was 10000 and 1000 N with the higher and lower spring stiffness, respectively, so that the static piston displacement was 0.25 mm in both cases.

The bi-directional explicit and implicit FSI coupling between Star-CCM+ and Abaqus were tested; these codes can be coupled without external middleware handling the communication between the codes. The two coupling methods were compared with each other and with the acoustic-structural FEM calculations.

Cell length in the CFD model was $\Delta x = 0.0125$ m, while the corresponding element length in the acoustic FEM model was $\Delta x = 0.02$ m. The larger element size in the acoustic model was considered sufficient since the acoustic calculation is considerably more accurate in the pressure transient modelling compared to the CFD calculation (see Pättikangas et al., 2011). Modelling of the compressible fluid in the CFD model was as described in the previous section. In the CFD model, time discretization was performed with the first order accurate two time-level method and single-precision machine accuracy was used. In the implicit CFD-FEM calculations, 5 FSI iterations inside time step were performed. The motion of the internal

CFD mesh due to the structural displacements is handled by the mesh morpher of Star-CCM+. The calculation parameters are listed in Table 2.

Table 2. Calculation parameters for solving the piston FSI problem.

Model	Δx [m]	$L/\Delta x$	Δt [μ s]	$CFL_c = c\Delta t/\Delta x$
CFD-FEM	0.0125	80	0.1 ... 5	0.008 ... 0.4
Acoustic-structural FEM	0.02	50	10	0.5

Figure 6 shows the piston displacement for the FSI calculations and for the piston without water for the case $m_s = 0.1m_f$. The fluid pressure field from the acoustic simulation at selected instants of time is shown in Fig. 5. When comparing the FSI solutions to the case of free piston, the effect of FSI is seen to be significant. The piston motion induces a pressure perturbation in the fluid which travels at the speed of sound and reflects from the fluid free surface. The explicit and implicit CFD-FEM calculations remain both stable and yield practically identical results. Agreement between the CFD-FEM and acoustic-structural models is fairly good, but some differences exist. These differences may be due to the large accuracy difference in the pressure transient modelling in the CFD and acoustic models.

Corresponding piston displacements for the case $m_s = 0.01m_f$ are shown in Fig. 7. The explicit CFD-FEM calculation with time step $\Delta t = 1 \mu$ s becomes unstable. The stability of the explicit FSI solutions commonly decreases with decreasing fluid compressibility (e.g. when moving from gas to liquid) or with decreasing ratio of structure density to fluid density (Causin et al., 2004; Abaqus, 2005; Timperi et al., 2006). When time step of the explicit calculation is decreased to $\Delta t = 0.1 \mu$ s, the calculation remains stable. The implicit calculation is seen to be stable even with a relatively large time step $\Delta t = 5 \mu$ s; computing time per time step becomes however somewhat longer than for the explicit calculation. Agreement between the stable CFD-FEM calculations and acoustic-structural calculation is fairly good also in this case.

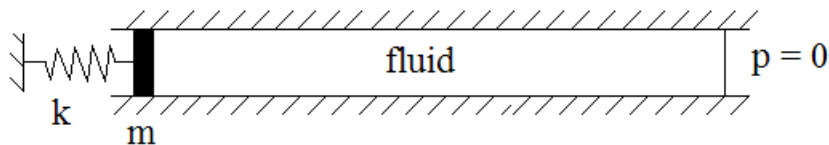


Figure 4. Piston FSI problem.

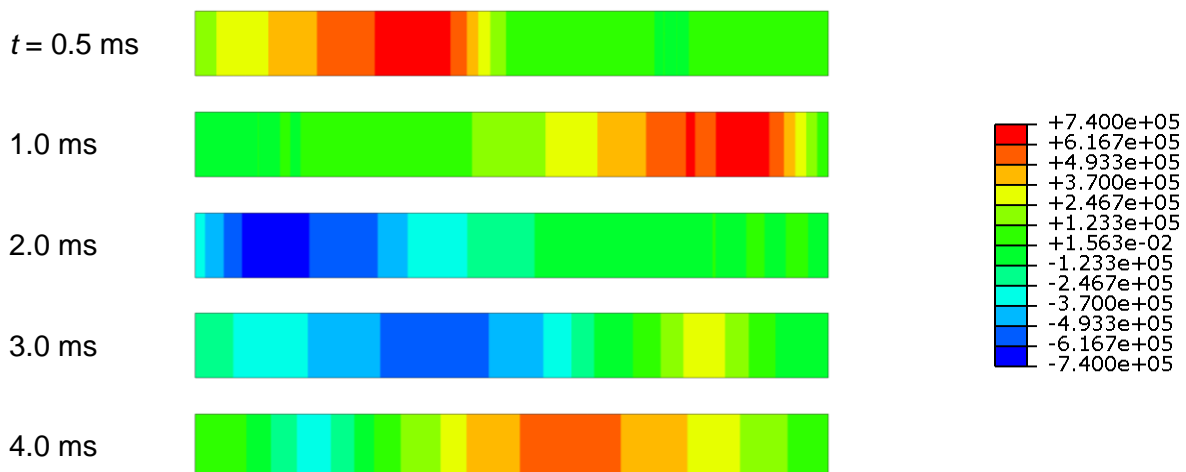


Figure 5. Piston fluid pressure field from acoustic simulation at selected instants of time for $m_s = 0.1 m_f$.

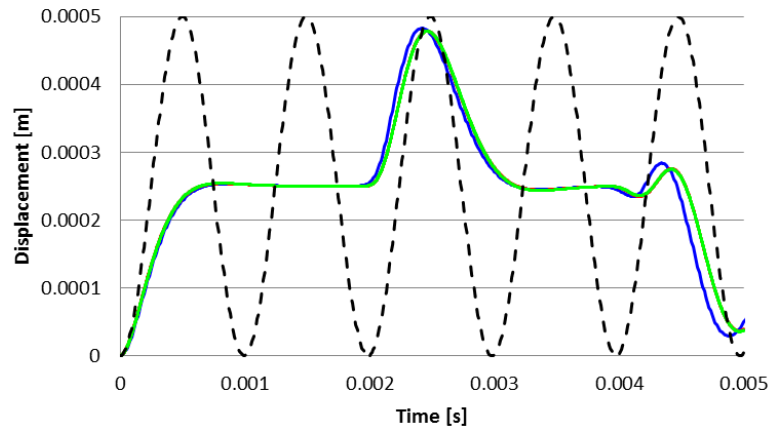


Figure 6. Piston displacement for $m_s = 0.1m_f$. (— Acoustic FEM $\Delta t = 10 \mu s$, — CFD-FEM explicit $\Delta t = 1 \mu s$, — CFD-FEM implicit $\Delta t = 1 \mu s$, -- No FSI)

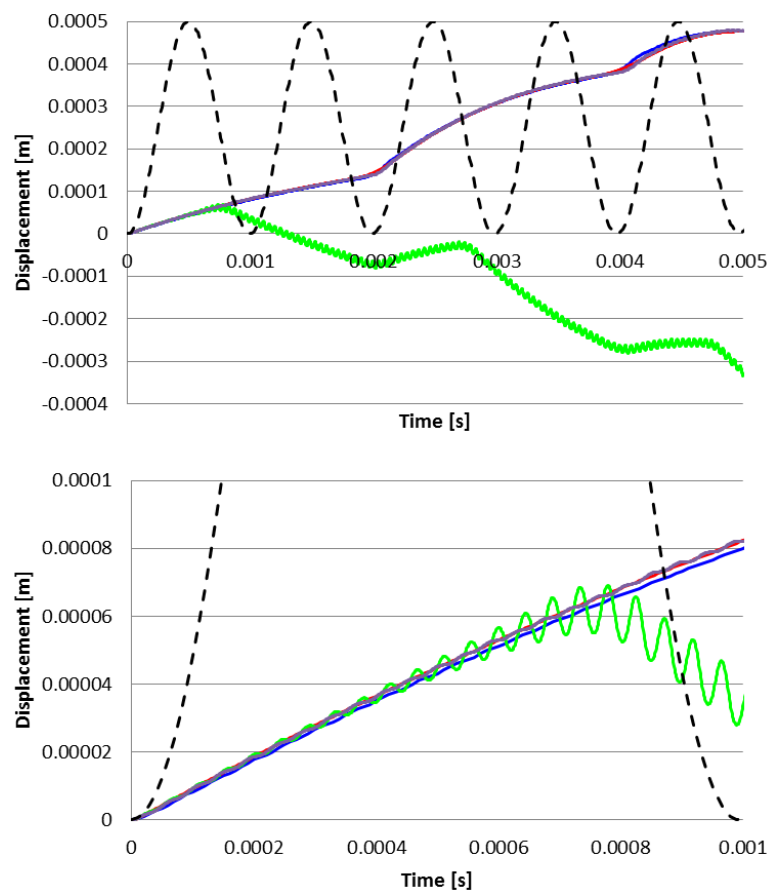


Figure 7. Piston displacement for $m_s = 0.01m_f$; zoomed axes are used in the lower plot. (— Acoustic FEM $\Delta t = 10 \mu s$, — CFD-FEM implicit $\Delta t = 5 \mu s$, — CFD-FEM explicit $\Delta t = 1 \mu s$, — CFD-FEM explicit $\Delta t = 0.1 \mu s$, -- No FSI)

2.3 Modelling of the PPOOLEX facility

The CFD mesh of the PPOOLEX facility is shown in Fig. 8. The mesh is same as used in previous studies (Pättikangas et al., 2009; Timperi, 2009) and contains about 136000 hexahedral cells. The Volume Of Fluid (VOF) model was used for tracking the free surface and the standard $k-\epsilon$ model and wall functions were used for modelling turbulence. Air was treated as compressible with the ideal gas law while water was assumed either incompressible or compressible. For compressible water, the speed of sound was set to $c = 1491$ m/s. The segregated flow solver with the SIMPLE pressure-correction algorithm was applied. Time discretization was performed with the second order accurate three time-level method. The PPOOLEX experiment SLR-05-02 (Laine and Puustinen, 2008; Puustinen et al., 2009) is considered, and hence a constant air mass flow rate of 805 g/s was set at the drywell inlet.

The structural model is same as used in the previous study (Timperi et al., 2014) and is shown in Fig. 8. It consists of about 15000 shell elements and of about 100 beam elements. Flexibility of the disc springs and base structures under the four vertical support columns were modelled with linear springs. Values $k = 21$ MN/m and $\gamma = 12$ kNs/m were used for the spring stiffness and damping coefficient, respectively. Values $\rho = 7850$ kg/m³, $E = 206$ GPa and $\nu = 0.3$ were used for density, Young's modulus and Poisson's ratio, respectively, in the steel structures. The Rayleigh damping parameter was set to $\beta = 5 \times 10^{-5}$. Implicit direct time integration was applied in the structural modelling.

Time step in the simulations was 0.2 ms. The number of iterations within time step in the CFD model was 10 and 20 in the cases with incompressible and compressible water, respectively. The numbers of implicit FSI iterations were same, since one FSI iteration per one inner iteration of the CFD model was performed. The motion of the internal CFD mesh due to the structural displacements was handled by the mesh morpher of Star-CCM+.

The VOF method of Star-CCM+ was found to be less stable than of Star-CD used earlier. The numerical problem occurred typically as the first bubble detaches from the vent pipe outlet, causing solution divergence. The divergence was found not to be related to FSI or moving mesh since it occurred similarly also without FSI, although including FSI increased the probability for divergence slightly. The problem could be prevented by shortening the time step from 0.5 ms to 0.2 ms, decreasing the Under-Relaxation Factors (URFs) of the segregated CFD solver and increasing the number of inner iterations.

Pool wall pressure in the simulation with incompressible water is shown in Fig. 9. The solution diverges quickly in spite of the implicit FSI algorithm. As mentioned above, low compressibility of the fluid typically promotes instability. The earlier simulations of the pool with explicit FSI algorithms have been severely unstable, and hence it is not surprising that the instabilities tend to arise even with an implicit algorithm when incompressible water is modelled. Stable calculations might be obtained by decreasing the time step and/or by adjusting URF of the FSI solution and performing more iterations within time step.

The rest of the simulations were performed with compressible water. The FSI solution remained stable with the default settings of the URF of the FSI solution, but pressure at the pool bottom wall showed considerable high-frequency oscillations, where the oscillation period corresponded to the time step size. By default, the URF is adjusted automatically based on solution convergence, with the maximum value being 0.5 and the minimum 0.2. The effect of the URF, number of iterations and whether Star-CCM+ or Abaqus leads the simulation was tested by running the simulation for 10 ms, i.e. 50 time steps. The number of iterations was varied by changing the number of inner iterations in the CFD model while keeping one FSI iteration per one inner CFD iteration. The fluid pressure signal at the pool bottom wall for the different test runs is shown in Fig. 10. Increasing the number of iterations and decreasing the URF seems to reduce the oscillations slightly. However, the best results

in this case are obtained simply by increasing the URF. The oscillations vanish almost completely when a constant URF of 0.7 is used. The effect of which code leads the simulation is quite negligible. It is noteworthy that even for the highly oscillatory FSI solution, low-pass filtered pressure signal and displacement signal at the pool bottom showed practically same results for the whole simulation period of 3 s as the non-oscillatory solution with proper URF.

Formation of the first bubble in the pool is shown in Fig. 11 for the experiment, for the earlier simulation with Star-CD (Pättikangas et al., 2010) and for the simulation with Star-CCM+. Charging of the drywell with air was found slower already in the earlier calculations, viz. the first bubble appears at the pipe outlet later in the calculations than in the experiment. Therefore, in the figures times between the calculations and experiment have been synchronized to the moment when the first bubble appears. The delays are about 0.39 and 0.32 s in the simulation with Star-CD and Star-CCM+, respectively. The exact cause for the delay is unknown. A delay in the mass flow sensor in the experiment was suspected earlier, but applying directly the measured drywell pressure as boundary condition in the CFD model decreased the delay only by about 0.1 s (Pättikangas et al., 2011). The bubble shape and rise velocity are slightly better in the simulation with Star-CCM+ than with Star-CD, although the same mesh is used. The simulation with Star-CD had a time step of 0.5 ms and first order time discretization, which cause lower accuracy compared to the simulation with Star-CCM+. In addition to the better time-accuracy of the Star-CCM+ simulation, the results may be affected also by better spatial discretization and improved VOF model.

Wall pressures and displacements are compared in Fig. 12. The Star-CCM+-Abaqus simulation shows qualitatively correct behavior but predicts too large displacements in the late phase. This may be caused by a resonance situation, since the simulation with rigid walls shows pressure oscillations with similar frequency as the natural frequency of the pool wall vertical motion. The earlier Star-CD calculations show lower pressure oscillations due to lower accuracy.

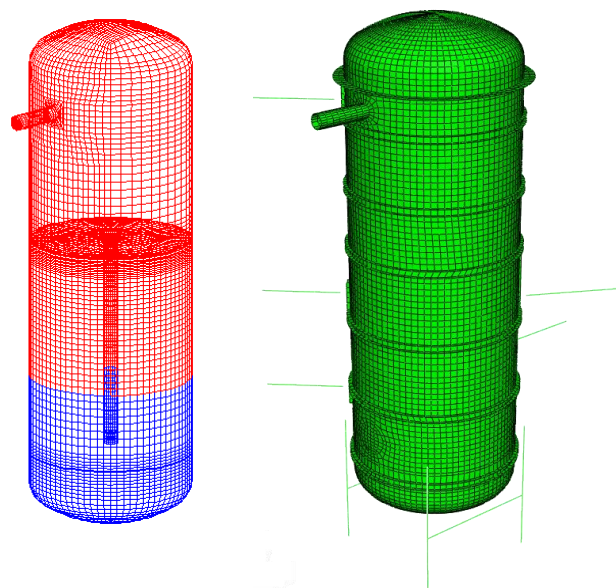


Figure 8. CFD (left) and FEM (right) meshes of the PPOOLEX facility.

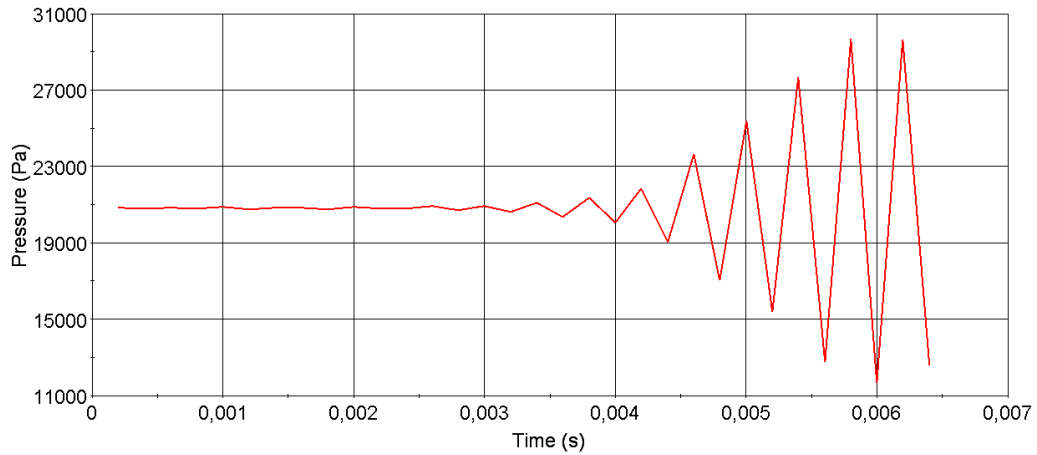


Figure 9. Diverging wall pressure at pool bottom in implicit FSI simulation with incompressible water.

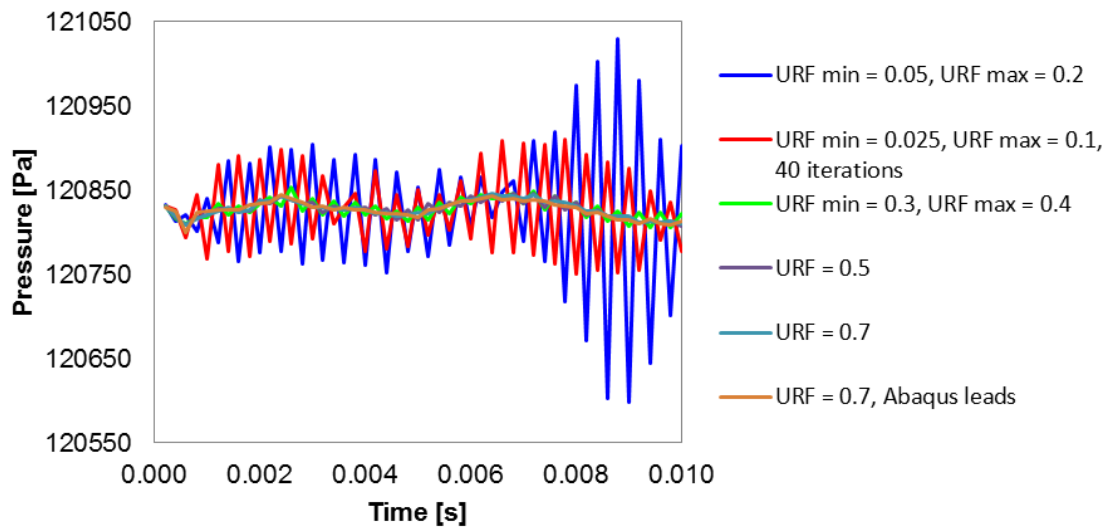


Figure 10. Effect of URF, iterations and simulation lead on the oscillatory pool wall pressure solution with compressible water.

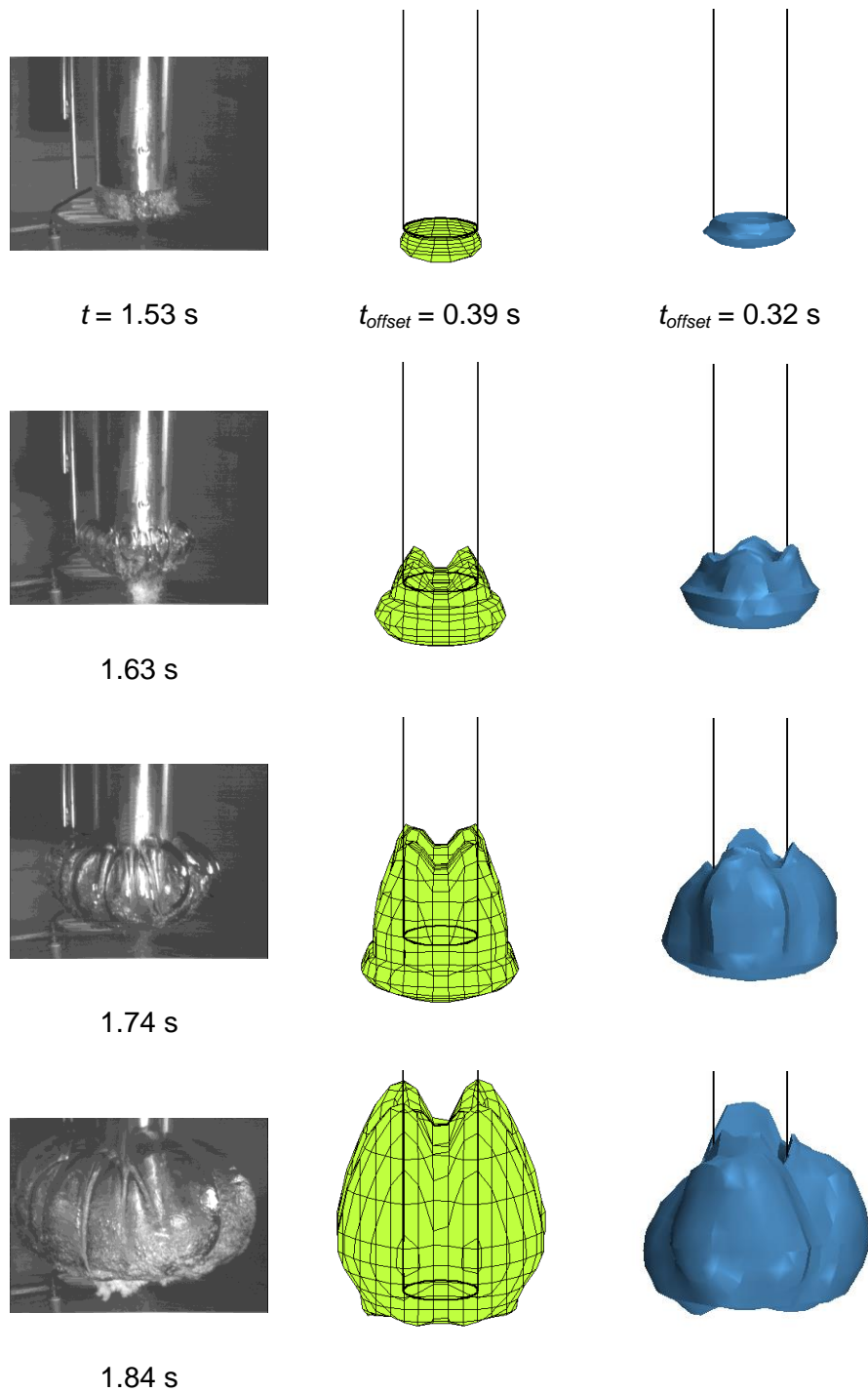


Figure 11. Air bubble at vent outlet in the PPOOLEX experiment (left) and in the calculations with Star-CD (middle) and Star-CCM+ (right).

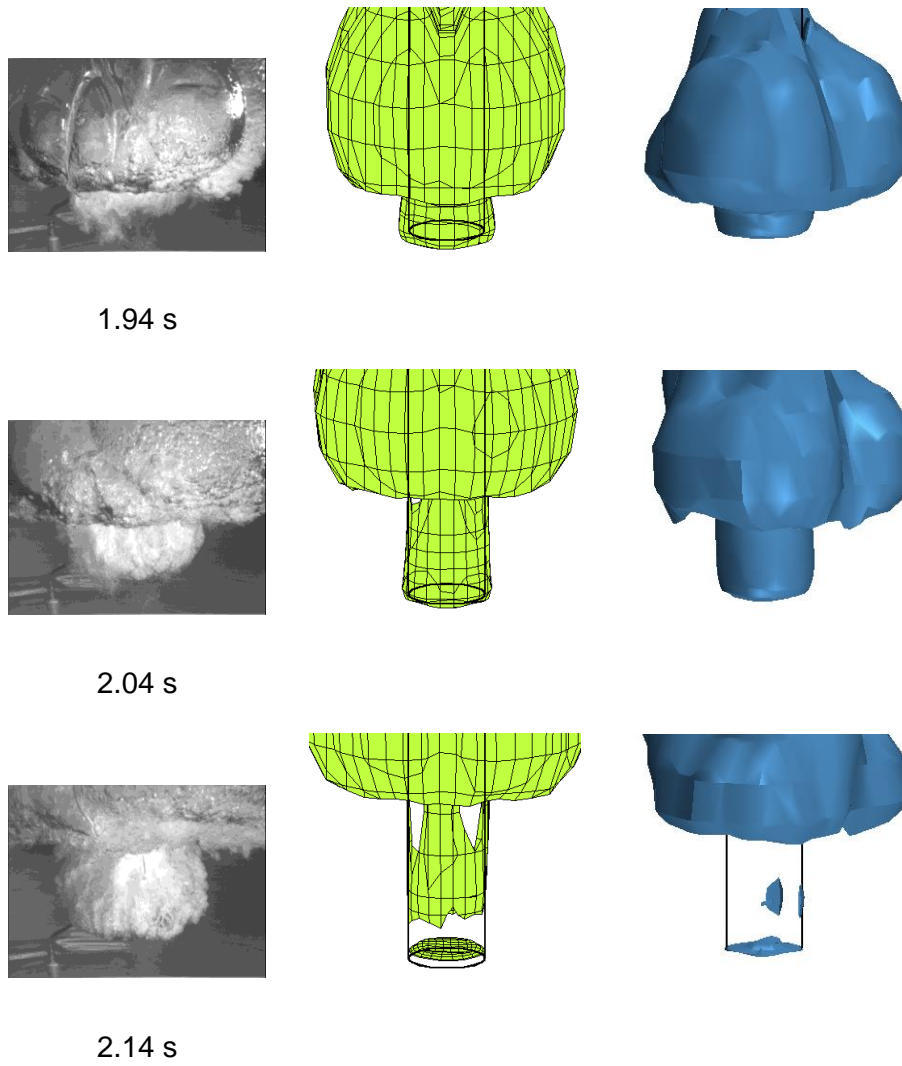


Figure 11. Continues from the previous page.

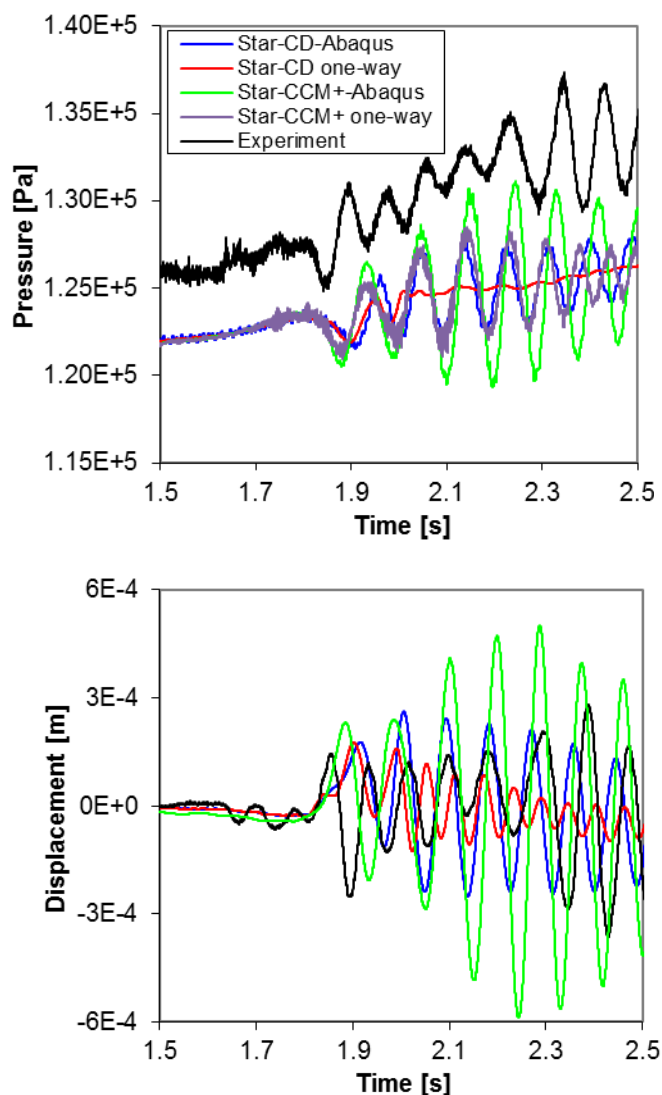


Figure 12. Wall pressure below pipe and bottom wall vertical displacement in the PPOOLEX experiment and in the calculations.

2.4 Modelling of a BWR containment

The CFD model of the BWR containment is shown in Fig.13. One sixteenth, i.e. 22.5° , of the containment was modeled so that the sector includes one of the sixteen blowdown pipes. Symmetry boundary conditions were applied at the sides. Even distribution of the pipes around the containment circumference was assumed here for simplicity. The CFD mesh had about 170 000 hexahedral cells. Only part of the drywell was modeled because a pressure boundary condition was used. The approximate boundary condition represents the drywell pressurization in case of a full break of the main steam line and is shown in Fig. 15; these pressures have been obtained from an earlier CONTAIN calculation. The VOF model was used for the free surface and the $k-\epsilon$ model and wall functions for modelling turbulence. The ideal gas law and the equation of state suitable for compressible liquid were assumed for the nitrogen and water, respectively. A speed of sound $c = 1491$ m/s was assumed for water.

The FEM model had about 5000 elements and is shown in Fig. 14. The upper water volumes of the containment were included as an acoustic fluid with two-way FSI coupling with the structure. The bottom of the model was fully fixed. For concrete, material properties $E = 39$

GPa, $\nu = 0.17$ and $\rho = 2400 \text{ kg/m}^3$ were used for elastic modulus, Poisson's ratio and density, respectively. For the steel cover above the reactor pressure vessel, values $E = 206 \text{ GPa}$, $\nu = 0.3$ and $\rho = 7850 \text{ kg/m}^3$ were used. For the acoustic water, values $K = 2.224 \text{ GPa}$ and $\rho = 1000 \text{ kg/m}^3$ were used for bulk modulus and density, respectively. This results in the speed of sound $c = \sqrt{K/\rho} = 1491 \text{ m/s}$. The damping ratio was set to 5% and 4% for the concrete and steel, respectively (Regulatory Guide 1.61, 2007). The Rayleigh damping was used and these damping ratios were adjusted to be exact for frequencies 10 Hz and 150 Hz.

The CFD and structural models are same as used in Pättikangas et al. (2010). Time step in the simulation was 0.25 ms. The number of iterations within time step in the CFD model was 15. The number of implicit FSI iterations was same, since one FSI iteration per one inner iteration of the CFD model was performed. The motion of the internal CFD mesh due to the structural displacements was handled by the mesh morpher of Star-CCM+.

Volume fraction of water in the pool is presented in Fig. 17 for the Star-CCM+-Abaqus simulation and for the earlier Star-CD-Abaqus simulation. The bubble shapes correspond quite well each other especially for the early time instants. It is noteworthy that the Star-CD model had a time step of 0.5 ms and first order time discretization, while the Star-CCM+ model has a time step of 0.25 ms and second order time discretization.

Pressures and displacements in the containment are shown in Figs. 18 and 19. The displacement output locations are shown in Fig. 16. The displacements are small particularly when considering the containment size. The small displacements are partly explained by the cylindrical containment shape with thick walls and by the sector symmetry. The effect of FSI is fairly small in this case. The Star-CD-Abaqus and Star-CCM+-Abaqus FSI calculations agree quite well with each other. The higher accuracy of time discretization in the Star-CCM+-Abaqus simulation is indicated by the somewhat higher oscillations in the pressures and displacements.

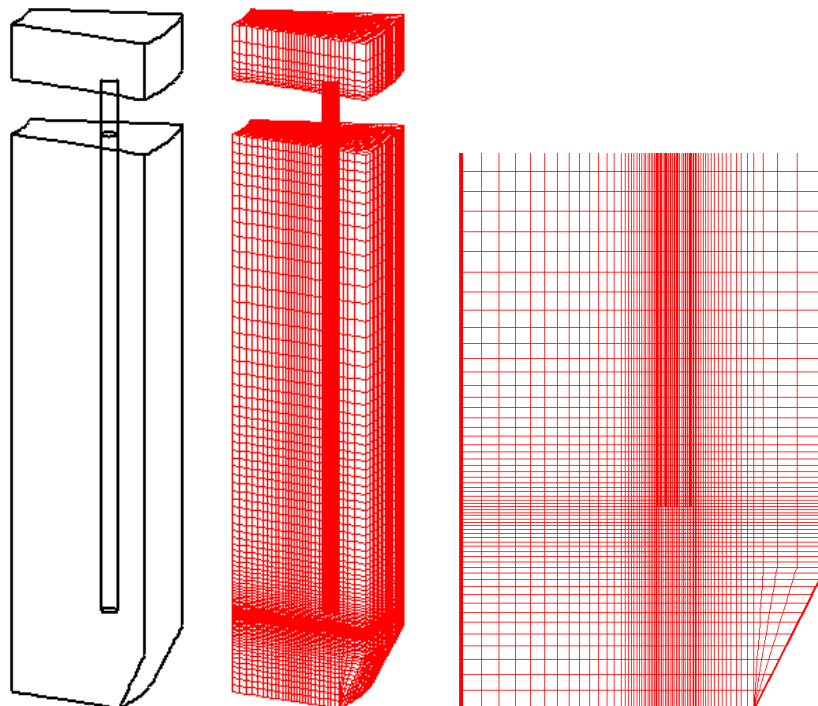


Figure 13. CFD geometry and mesh of the BWR containment.

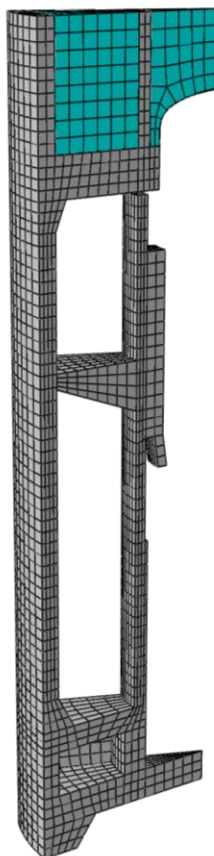


Figure 14. FEM mesh of the BWR containment.

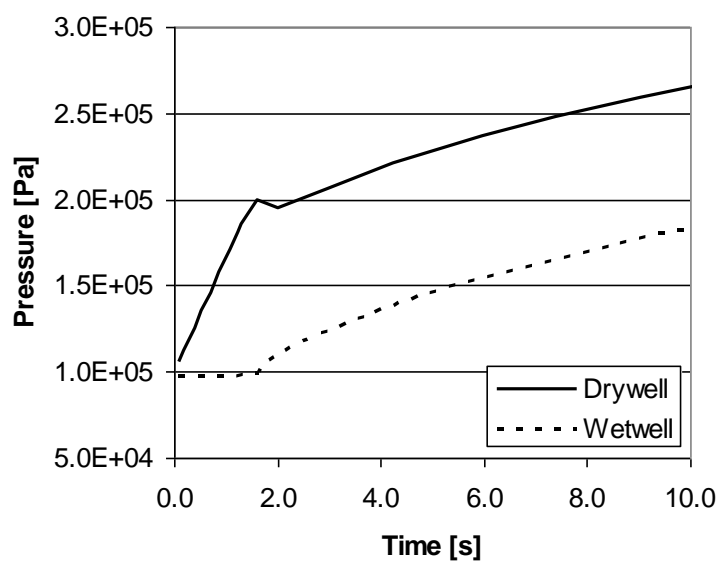


Figure 15. Gas pressure in the BWR drywell and wetwell in the early phase of steam line break. The drywell pressure is used as a boundary condition in the CFD model.

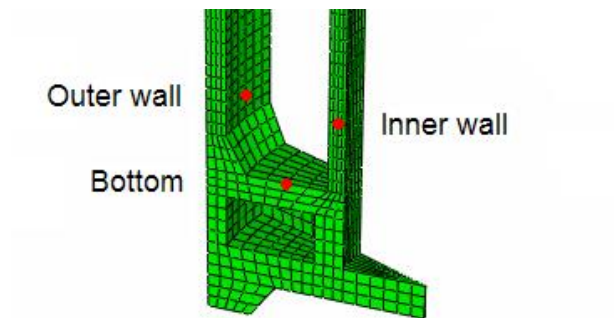


Figure 16. Locations of displacement output for the BWR structural model.

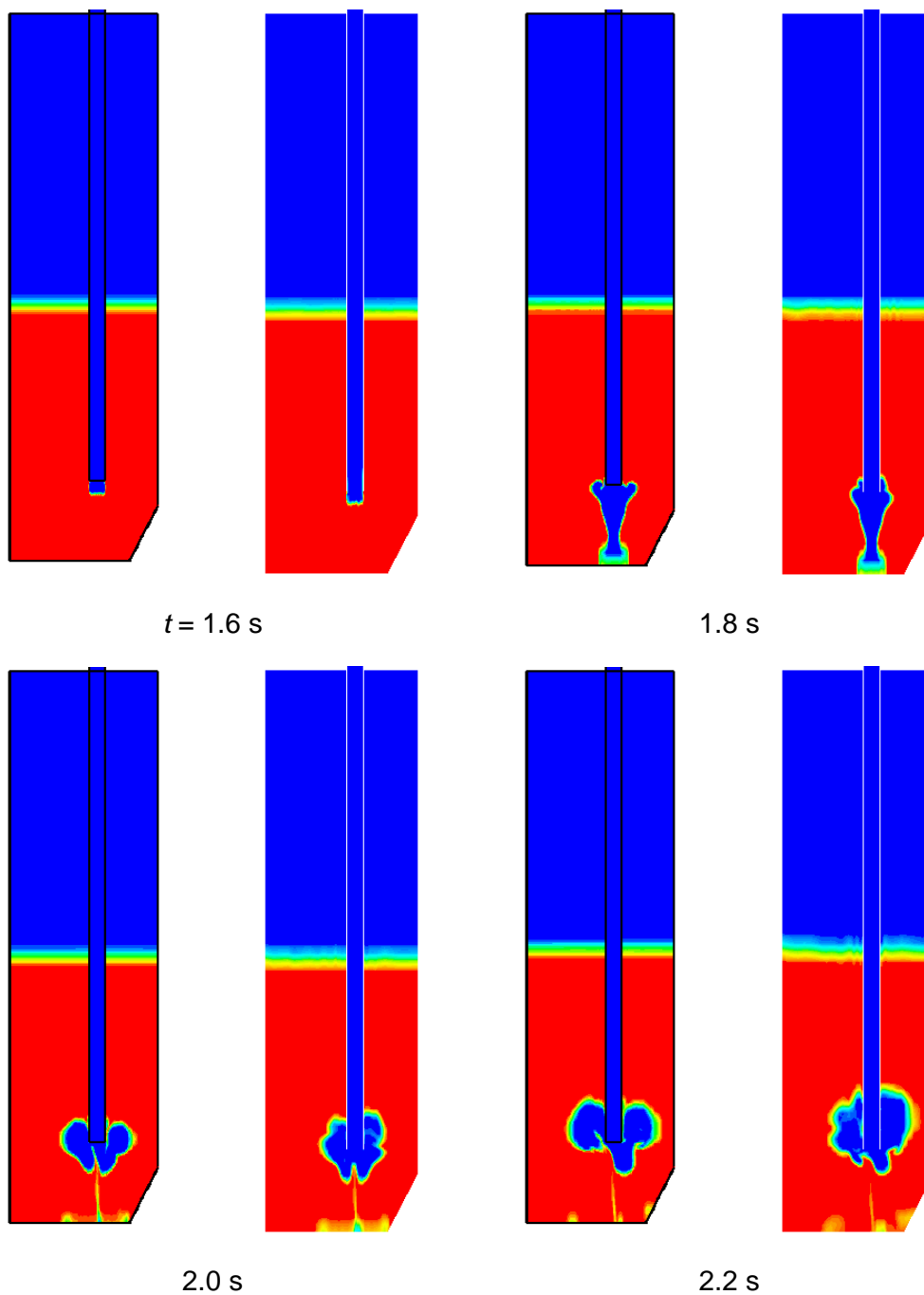


Figure 17. Volume fraction of water in the BWR containment for calculations with Star-CD (left plots) and Star-CCM+ (right plots).

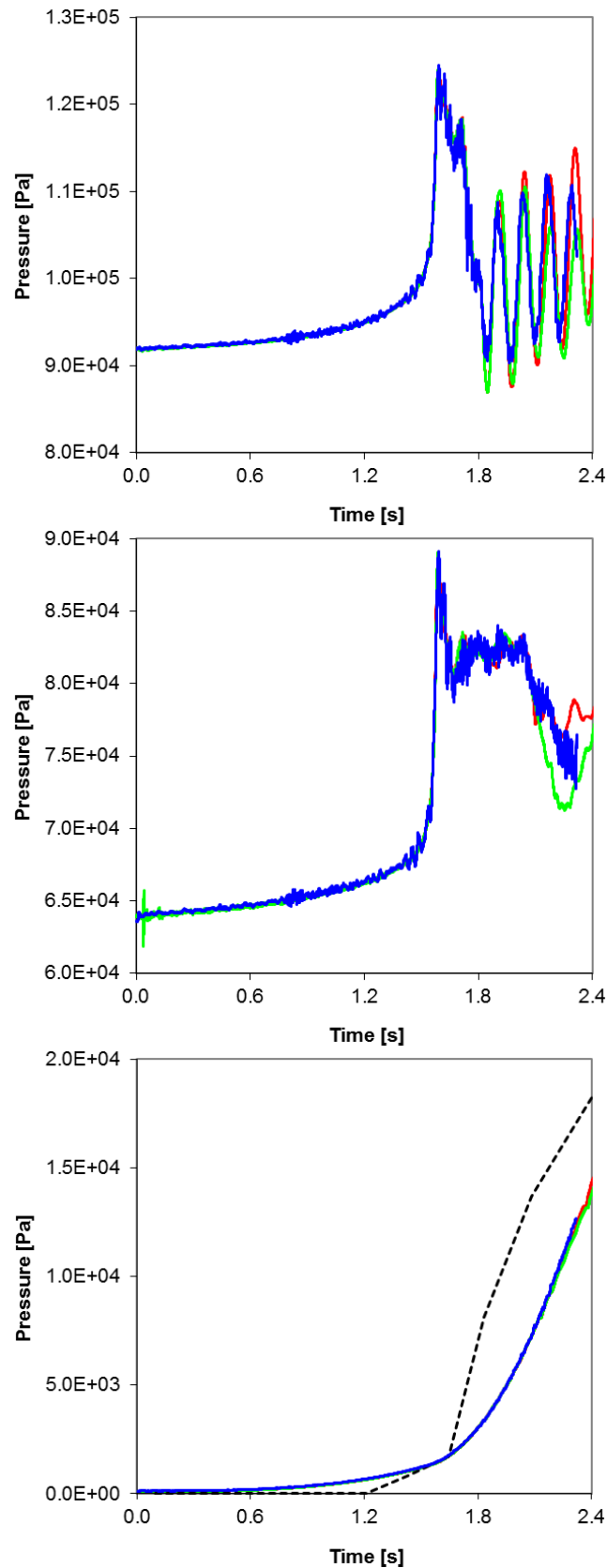


Figure 18. Pressures in the BWR containment. From top: center of pool bottom, outer wall at pipe outlet level, wetwell gas. (— Star-CCM+-Abaqus two-way implicit, — Star-CD-Abaqus two-way explicit, — Star-CD-Abaqus one-way, -- CONTAIN calculation)

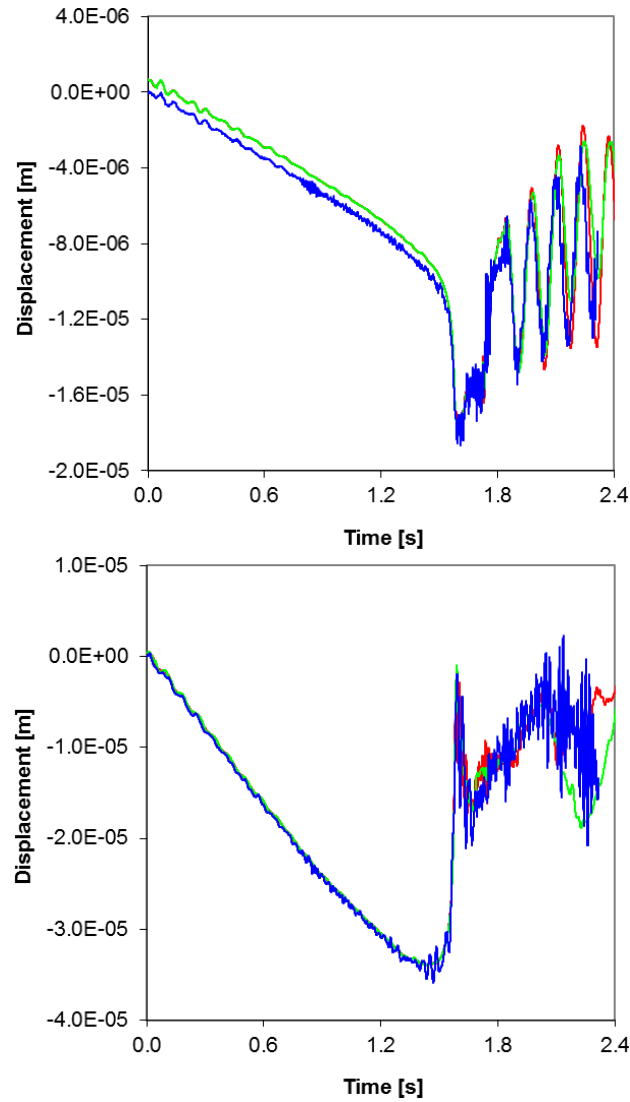


Figure 19. Displacements in the BWR containment. Upper: vertical displacement at location "Bottom", lower: radial displacement at location "Outer wall". (— Star-CCM+-Abaqus two-way implicit, — Star-CD-Abaqus two-way explicit, — Star-CD-Abaqus one-way)

3. Simulation of BWR containment with acoustic FSI model

Mesh sensitivity studies, convergence of statistics and material damping investigation of the Abaqus model were carried out in the previous work (Timperi et al., 2014). In this work the same model is used, where main focus is on further development of the stochastic simulations of the BWR containment. Previously, only stochastic simulation of chug event desynchronization was considered, whereas in this work the statistics are expanded to load signal length and amplitude. The load signal shape used in this study is Case 3 load shape from section 4.4 of Timperi et al. (2014).

3.1 FEM model of the BWR containment

The FEM model of the BWR containment with 16 vent pipes has been simplified as shown in Figure 20. Four different element types have been used in the model. The total number of elements is 21715, including 8032 linear hexahedral acoustic elements (Abaqus element type AC3D8R), 12173 linear hexahedral continuum elements (C3D8R), 1508 linear hexahedral continuum shell elements (SC8R) and two mass elements. The solution was carried out by explicit direct time integration method. A density of 2400 kg/m^3 , elastic modulus of 39 GPa and Poisson's ratio of 0.17 are set for concrete material. The water density is set 1000 kg/m^3 . The FSI analyses are carried out with sonic velocities of 450 and 1412 m/s, which are chosen according to Björndahl and Andersson (1998).

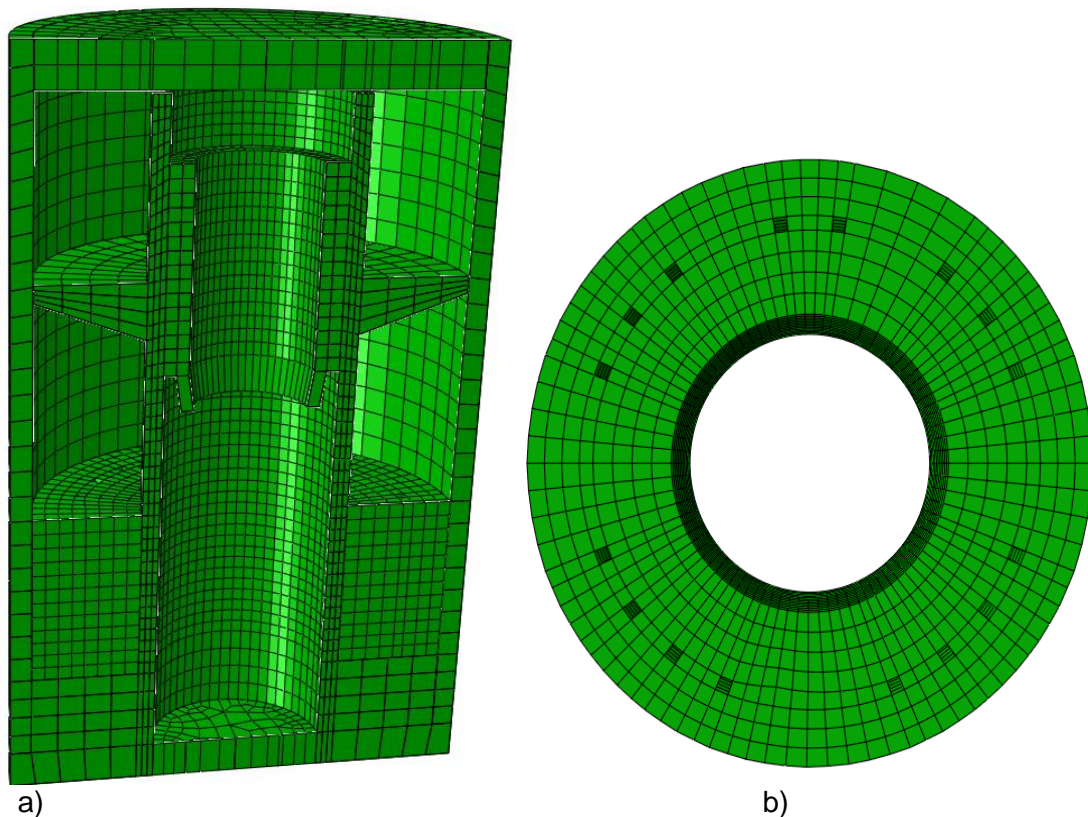


Figure 20. Meshed model of simplified BWR containment. a) Model cut in half for visualization with concrete structure and water. b) Wetwell water with simplified 16 square shaped vent pipe cross-sections.

As it was found from the previous study (Timperi et al., 2014), the structural response was more sensitive to the water sonic velocity than the detailed load shape. Thus, in this work further stochastic implementation of loads have been considered by using a single load shape.

3.2 Stochastic load amplitude (Case 1)

In the previous study (section 4.5 p. 34 in Timperi et al., 2014), desynchronization between chug events was studied statistically with mean value of zero and standard deviation of 0.042 s. In this section, in addition to the desynchronized time, load amplitudes are also applied statistically, i.e. the load amplitude varies randomly with given mean value and standard deviation. The normalized load amplitude mean value and standard deviation are computed from Fig. 8 of Kukita and Namatame (1985). From the resulted mean value of 1 unit and standard deviation of 0.233 units the following normal distribution curve was generated in Matlab.

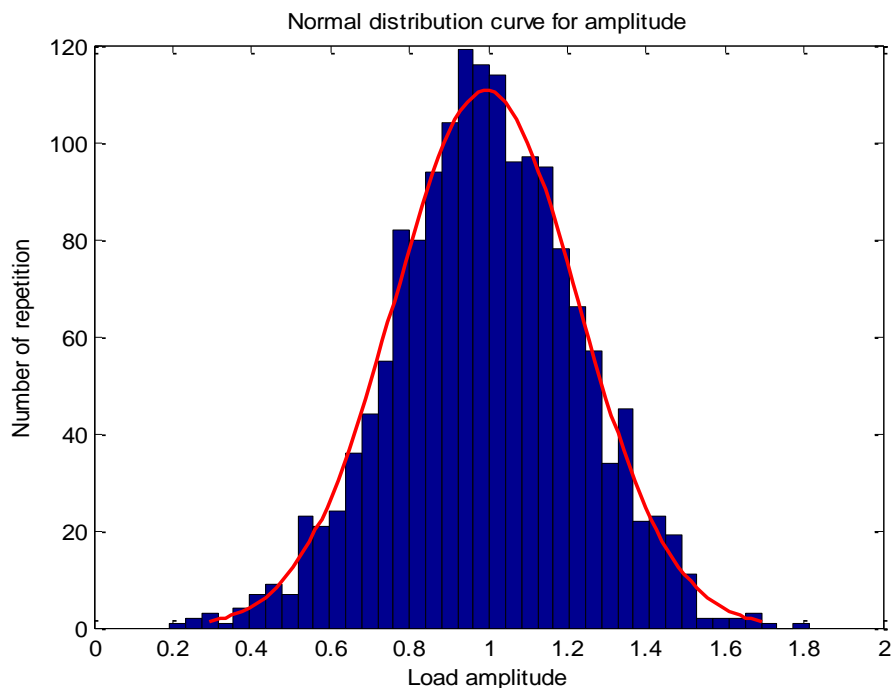


Figure 21. Normal distribution curve for the normalized load amplitude

There are totally 16 vent pipes in the model, 100 chug events are performed, and average time between each chug event is 2s. Thus, altogether all pipes are loaded 1600 times. From Figure 21 it can be seen that the pipes are loaded with amplitude of 1 unit about 110 times. Based on the given mean value and standard deviation, Matlab randomly chooses amplitudes.

By comparing Figures 23a and 23b, it can be seen that amplitudes in Figure 23b are fluctuating for each pipe randomly, while in Figure 23a amplitudes are constant.

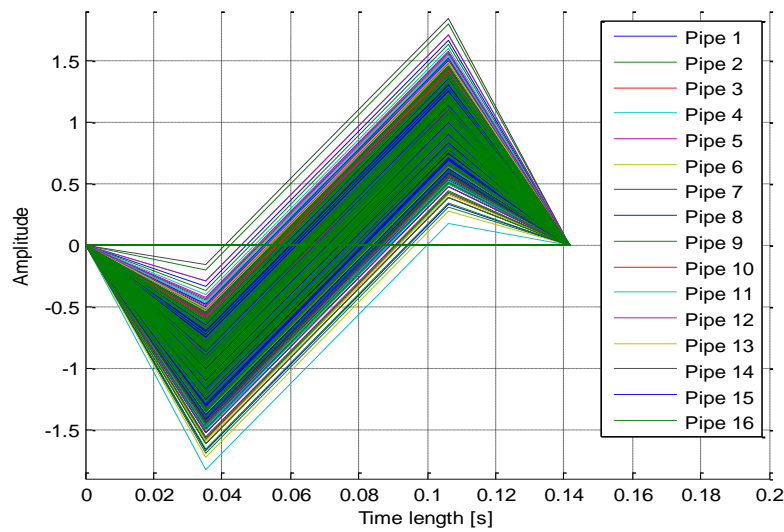


Figure 22. Randomized load amplitude for 1600 load times. Chosen load shape is from Case 3 of Figure 30 of Timperi et al. (2014).

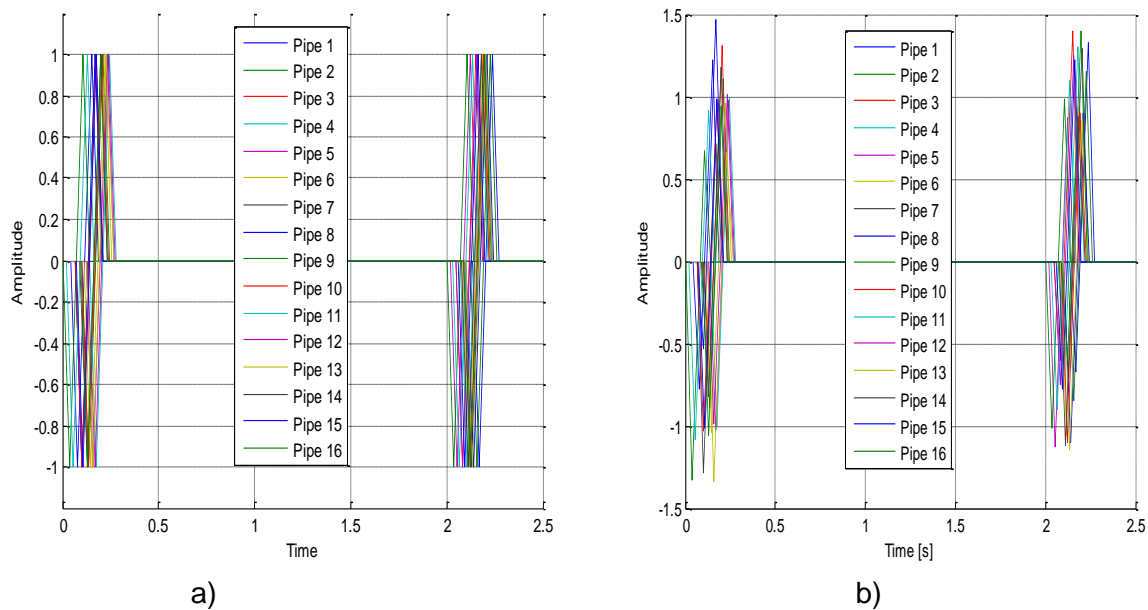


Figure 23. Load amplitude for 16 vent pipes in two chug events. a) Desynchronized chugging from the previous study. b) Desynchronized chugging and randomized load amplitude with mean value of unity and standard deviation of 0.054 units.

3.3 Stochastic load period (Case 2)

In Case 2, desynchronized chug events and stochastic load period length implementations are considered. From the seven vent pipe experiment in Fig. 4 of Kukita and Namatame (1985) standard deviation through normalization approach for the considered load shape is computed. The mean value of the load period is 0.14165 s, which corresponds the period of the load shape from previous study. Standard deviation of 0.01399 s is computed for the load period. The same way as in section 2.2, all the pipes have been loaded altogether 1600 times (each pipe 100 times) in a time period of approximately 200 seconds. Normal

distribution curve for the given standard deviation and mean value is generated in Matlab as shown in Figure 24. It should be noted that the determined standard deviation of the load period length is highly approximate.

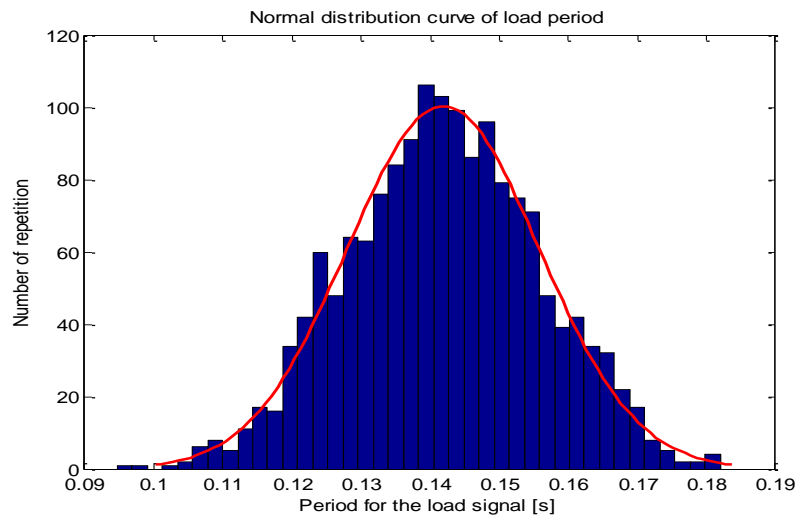


Figure 24. Normal distribution curve for the load period.

According to the given mean value and standard deviation, Matlab randomly picked the load period for 1600 runs in Figure 24. Figure 25 shows loads shape for 1600 randomized load periods.

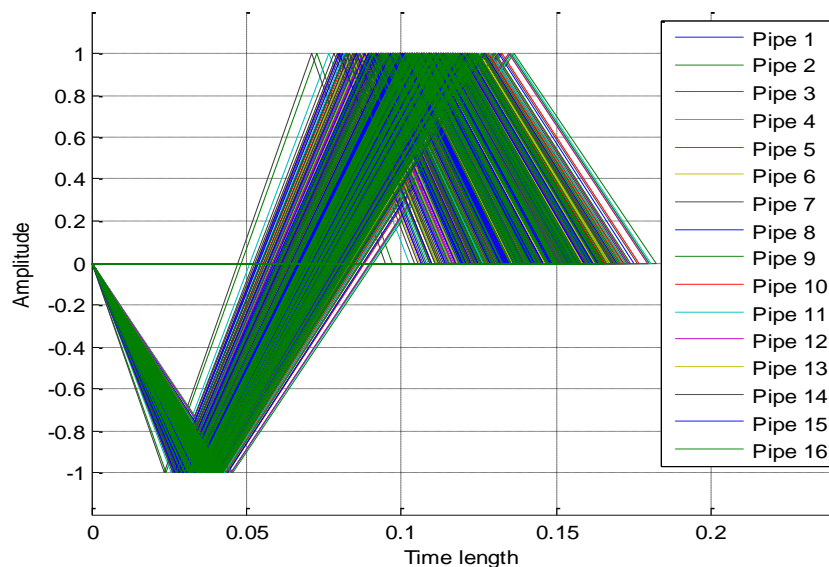


Figure 25. Load shape for 1600 randomized load periods.

From Figure 25, the smallest random load period is 0.09465 s for the pipe 14 and the largest load period is 0.182 s for the pipe 7.

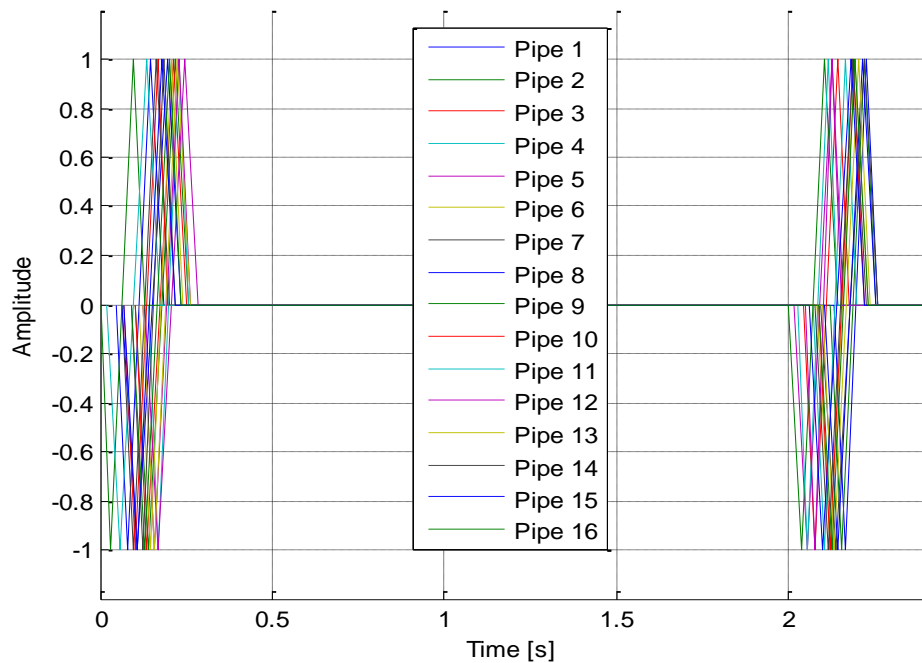


Figure 26. Load shape for 16 vent pipes in two chug events. Statistically desynchronized chug events and load period.

By comparing Figure 23a and Figure 26, following differences can be observed: in Figurea loading of each pipe starts randomly, while load period stay constant for all pipes, however, in Figure load periods also change randomly for all pipes.

3.4 Combination of all three statistics (Case 3)

In this section, the objective is to apply loads in the BWR containment FEM model as realistically as possible. Thus chug event starting times, load amplitudes and load periods are randomized with the given mean values and standard deviations. For the sake of comparison, for load amplitudes and load periods the same normal distribution curves generated by Matlab in Figures 21 and 24 will be used. The same desynchronized data, generated in the previous work (Timperi et al., 2014) with standard deviation of 0.042 s and mean value of 0 s will be used as well. Figure 27 shows combination of randomized load amplitude and load period for 1600 loadings.

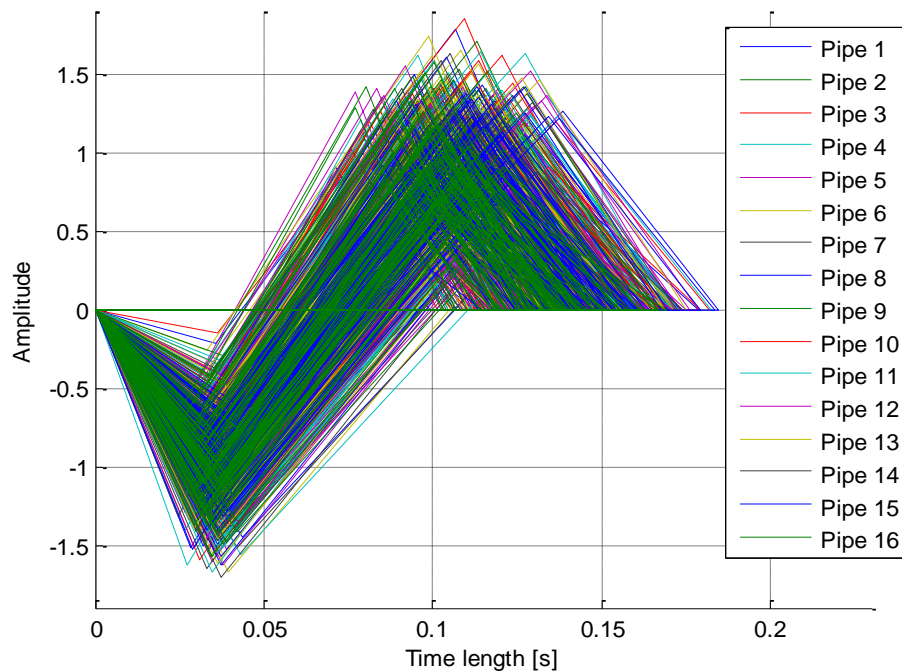


Figure 27. Statistically randomized load amplitudes and periods.

It must be noted that mean values and standard deviations of randomized load amplitudes and periods are independent of each other. In Figure 27 the third randomization, which is desynchronization between chug events, is not presented. In order to be able to present all three statistics graphically together, two chug events are presented in Figure 28.

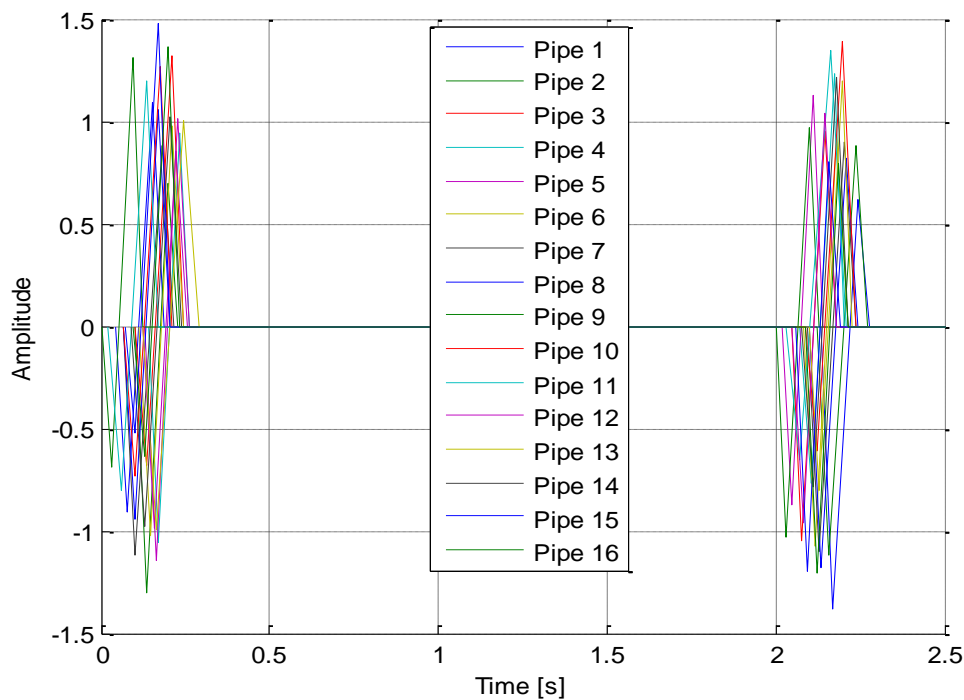


Figure 28. Statistically randomized chug event starting times, load amplitudes and load periods.

In Figure 28 average time between chug events is 2 s. In Figure 28, which represents the Case 3 loading, chug events desynchronization, load amplitudes and load periods are randomized.

3.5 Comparisons of the results from all three cases

For comparison of the results between different cases and the results from the earlier study (Timperi et al., 2014), same node set is chosen as in the previous study. At the selected node set, statistics of horizontal displacement magnitudes are calculated and averaged over nodes for comparing the different cases. Figure 29 shows the selected node set.

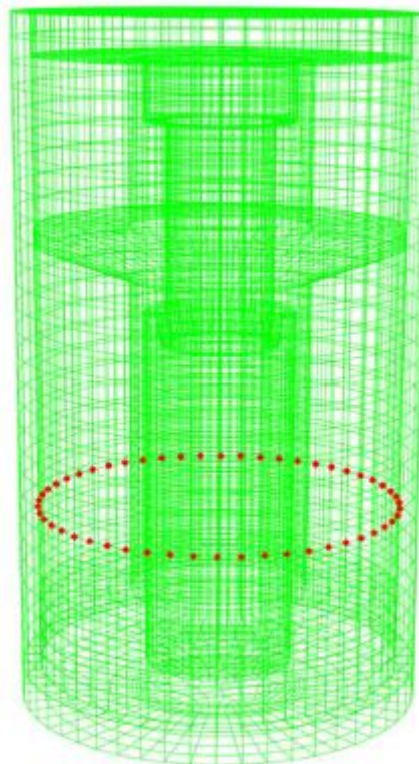


Figure 29. Nodes set for gathering displacement statistics at the inner surface of BWR containment.

Figures 30 and 31 are plot of root mean squared (RMS) and maximum horizontal displacement magnitudes respectively, where a single load shape with two water sonic velocities 450 and 1412 m/s are used. Both Figures 30 and 31 are normalized with respect to maximum values, Case 0 in both figures presents the results from the previous study (Timperi et al., 2014). For sonic velocity of 450 m/s, the highest displacements occur in Case 2, where desynchronization time and load periods are randomized. Highest displacements at sonic velocity of 1412 m/s occur in Case 3, where desynchronizations time, load amplitudes and load periods are randomized. As can be seen from the figures, sonic velocities have major effect on the structural response.

Note that if the random amplitude cases are compared to a case with constant amplitude set according to the maximum experimental value, then the more realistic cases with amplitude variation result in lower stresses compared to the constant amplitude case.

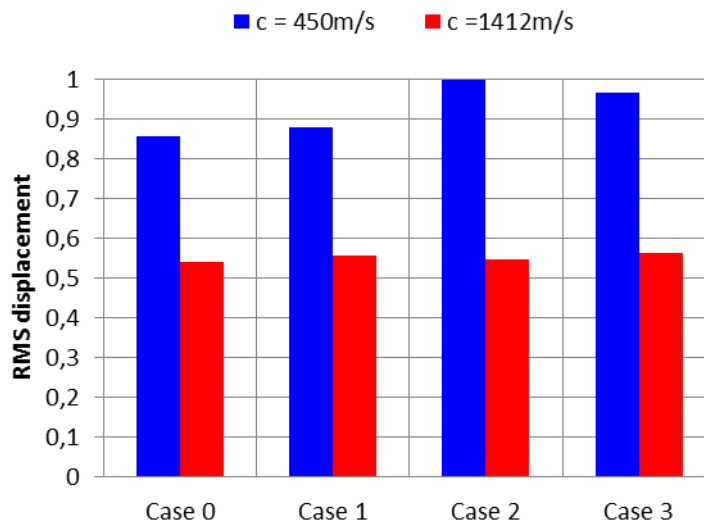


Figure 30. Normalized RMS horizontal displacement for four different statistical cases with the single load shape.

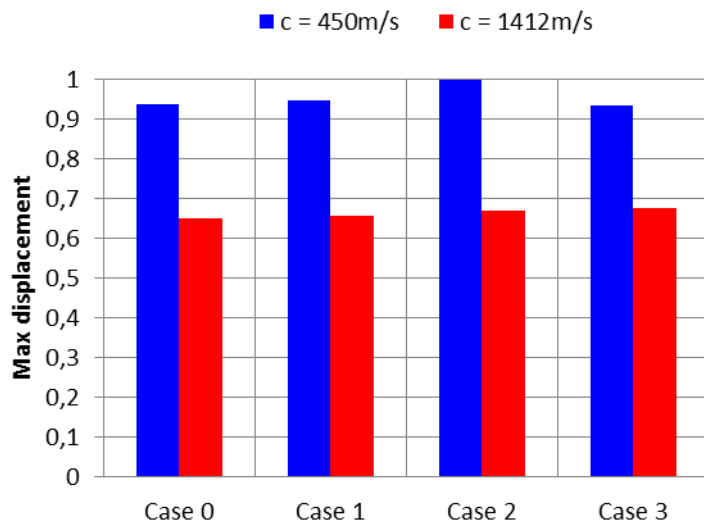


Figure 31. Normalized maximum horizontal displacement for four different statistical cases with the single load shape.

Figure 32 presents deformations and stresses distributions from FEM simulation of BWR containment at selected instances of time for the Case 3 and sonic velocity of 450 m/s. Note that since unit loading is used due to the model linearity, the presented absolute magnitudes are not realistic.

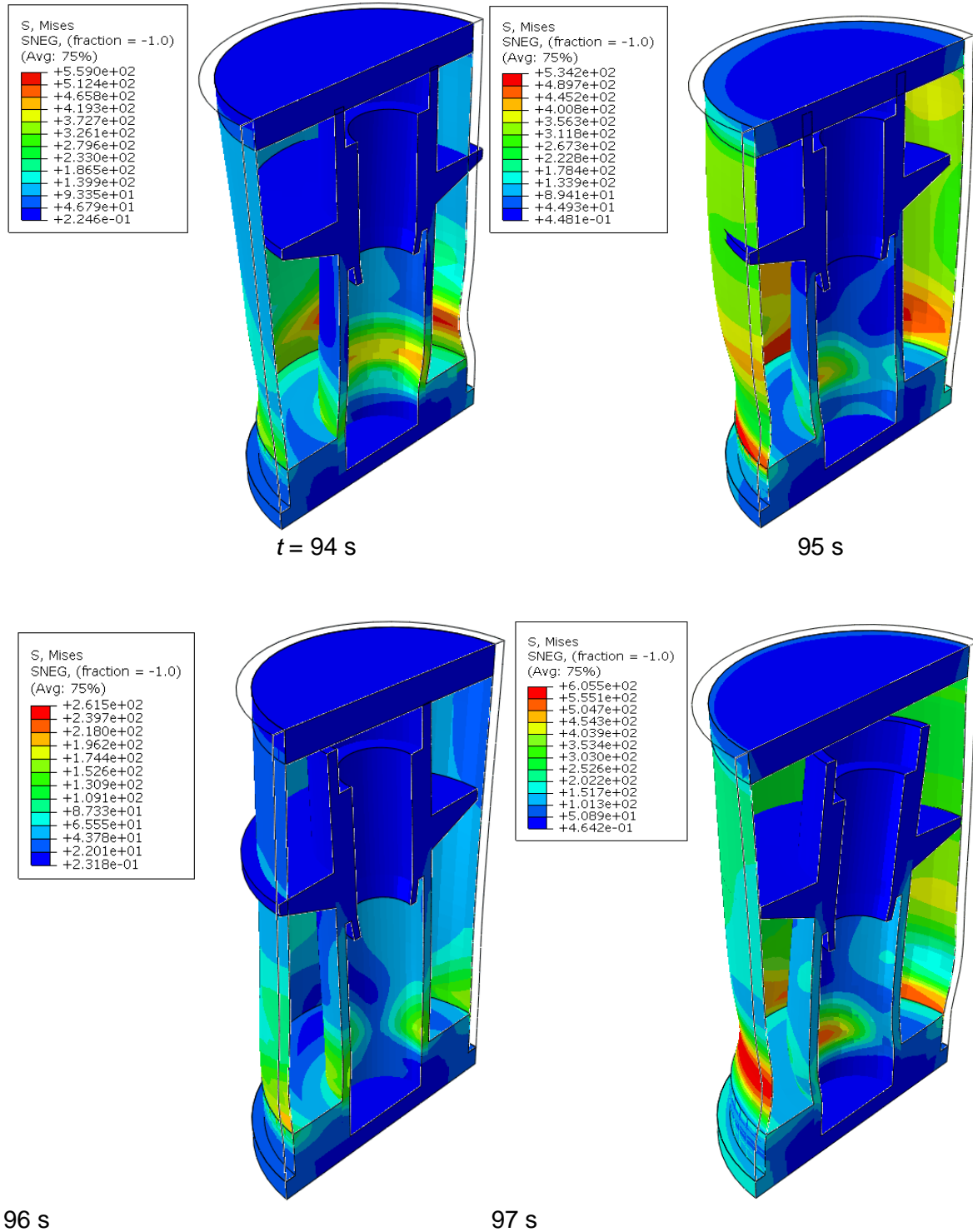


Figure 32. Von Mises stress distribution (Pa) and deformations in the BWR containment with single load shape and stochastic load desynchronization, amplitude and period. Unit loading has been used and deformations are scaled up by 7×10^6 .

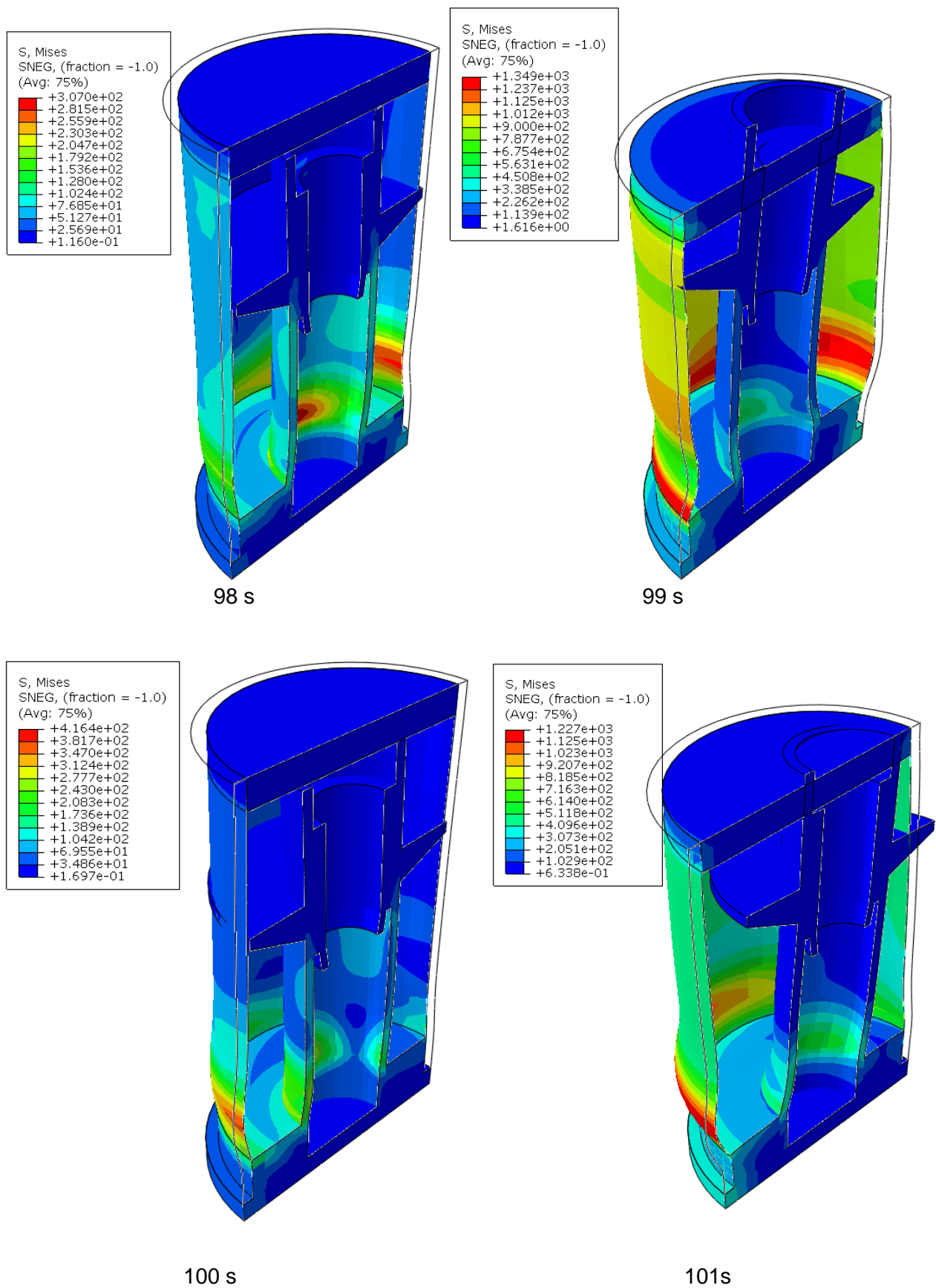


Figure 32. Continues from the previous page.

4. CFD calculations of blowdown in a BWR containment

Two different approaches exist for solving two-phase flow of gas and liquid. In the Volume Of Fluid (VOF) model, the interface between the immiscible liquid and gas is tracked during the simulation. The interface is kept sharp with a numerical algorithm in order to reduce the effect of diffusion and to avoid mixing of the phases. In the Euler-Euler method, mixture of small gas bubbles and continuous liquid phase is considered, but the interface of the bubbles and the liquid is not solved in detail. Instead, the volume fraction of the bubbles in each grid cell is solved from so called two-fluid equations, where continuum approximation is used for the flow of small bubbles.

In modelling of the behavior of large steam bubbles during blowdown of vapor into water pool, both tracking the surface of large bubbles and the volume fraction of small bubbles would be beneficial. Therefore, a hybrid method of VOF and Euler-Euler method would be useful, where the interfaces of large bubbles are tracked but only volume fraction of small bubbles is solved.

Laviéville (2008) and Coste (2013) have introduced the Large Interface Model, where “large” interfaces between the phases are resolved. In the following, the possibility of combining the Large Interface Model with the Euler-Euler model of ANSYS Fluent is first discussed. Results on applying the model to PPOOLEX experiments are briefly described. Then, results on modelling the initial stage of postulated large-break LOCA in BWR by using the VOF method are discussed.

4.1 Large Interface model

In the Large Interface model, the numerical mesh of the CFD model is scanned and the grid cells at the “large interfaces” between the phases are determined. Then, the direction of the normal of the interface is resolved and the grid cells adjacent to the interface are located. The idea of the method is illustrated in Fig. 33. The model equations and the implementation of the method were summarized earlier by Pättikangas et al. (2014).

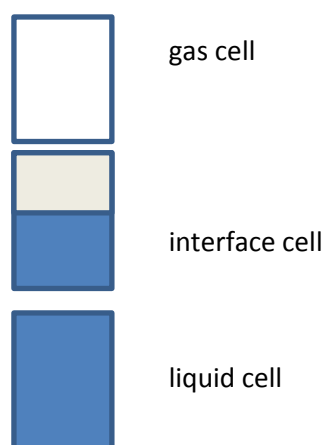


Figure 33. A three-cell stencil for describing interface of the phases in the Large Interface model.

The Large Interface method has been implemented in the ANSYS Fluent 15.0 code by using User-Defined Functions (UDF) of Fluent. Test simulations of PPOOLEX experiments have been performed by using the method and some examples were presented earlier by Pättikangas et al. (2014). In the simulations, the method has not so far been stable enough for practical calculation of nuclear reactor safety assessment. The method could not be made stable enough by using only User-Defined Functions. Access to the full source code of the solver would have been beneficial.

In the following, CFD results for BWR containment are shown, where the VOF method of ANSYS Fluent is used.

4.2 CFD model for a sector of a BWR containment

The CFD model is shown in Fig. 34, where the model geometry is shown on the left. The model consists of a 90° sector of the dry well and wet well compartments, which contain four vent pipes with diameters of 60 cm. The water level in the wet well compartment is shown on the left, where the submergence depth of the vent pipes is 6.8 m.

The numerical mesh, which contains about 2.8 million grid cells, is also shown in Fig. 34. Most of the cells are located in the wet well compartment and the mesh is refined near the vent pipes. Details of the mesh are shown on the right in Fig. 34, where the bottom part of the dry well and the bottom of the wet well can be seen. In the 90° sector model, symmetry boundary conditions are applied for the flow field on the planes located at 0° and 90°.

A postulated Large-Break Loss-Of-Coolant Accident (LB-LOCA) was studied with the numerical model. In the dry well compartment, a mass source of 800 kg/s of gas with a temperature of 160 °C was assumed. The mass source was located in a region having a volume of about one cubic meter in the dry well compartment. Initially, the dry well and the gas space of the wet well were filled with nitrogen having temperature of 27 °C and pressure of one bar. The temperature of the water was also 27 °C. Nitrogen was treated as ideal gas and compressible liquid model was used for water.

The Volume Of Fluid model of ANSYS Fluent 16.0 was used in the simulation. The interface of the phases was modelled as sharp, and the implicit body force formulation was used for the buoyancy terms. The turbulence was modelled with the standard $k-\varepsilon$ model by using standard wall functions. The time step was 1 ms, and only the early stage of the gas discharge from the dry well to the wet well was calculated. In the simulation of the first 10 s of the discharge, 10 000 time steps were needed. The simulation took about three weeks with a computer having 16 CPU cores.

4.3 CFD calculation of the early phase of Large-Break LOCA

In the following, the results of the model simulation of the early phase of Large-Break LOCA are summarized. The results for the void fraction, pressure and flow velocity are illustrated in the contour plots in Figs 35–38. The results are plotted on the cylindrical surface, which contains the axes of the four vent pipes.

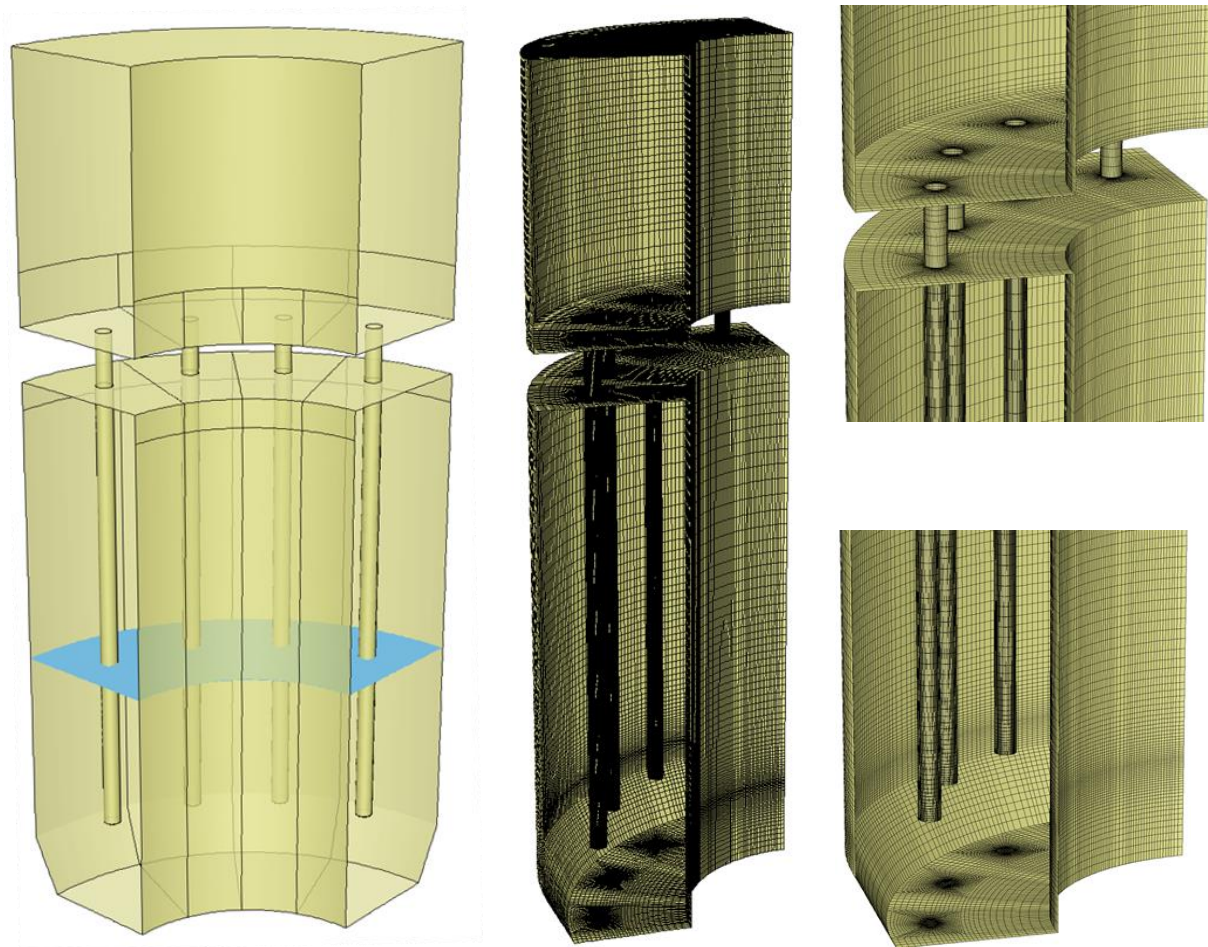


Figure 34. Geometry of the CFD model (left) and the surface mesh (center) and details of the top and bottom parts of the mesh (right).

In Fig. 35, the void fraction is shown at different instants of time. The clearance of the four vent pipes occurs almost simultaneously at time $t = 2.2$ s. The velocity of the water plug expelled from the vent pipe is somewhat above 8 m/s, and some nitrogen gas follows the water plug to the bottom floor of the wet well. Some traces of this gas can be seen near the pool bottom at time $t = 2.5$ s, where the first gas bubbles have formed at the outlets of the vent pipes.

When the first bubbles have formed, they start rising upwards and the bubbles break the water surface at time $t = 4.8$ s. The holdup of gas in the water pool has elevated the water surface. When the gas bubbles break into the gas space of the wet well, the elevated water collapses downwards causing pressure load on the bottom part of the wet well.

New bubbles are formed at the outlets of the four vent pipes in fairly synchronous manner. Some differences between the vent pipes can, however, be observed. When bubbles are detached at the outlets of the vent pipes, some water penetrates into the pipes at times $t = 5.5$ s, 7.5 s and 10 s. The period of this phenomenon is about two seconds and it occurs even though the gas in the vent pipes is non-condensable.

In Fig. 36, the three-dimensional surfaces of the first bubbles are shown. The iso-surfaces of void fraction $\alpha = 0.2$ are plotted at a few instants of time. The formation of the bubbles, their detachment from the outlets of the vent pipes and the rise of the bubbles to the water surface can be seen.

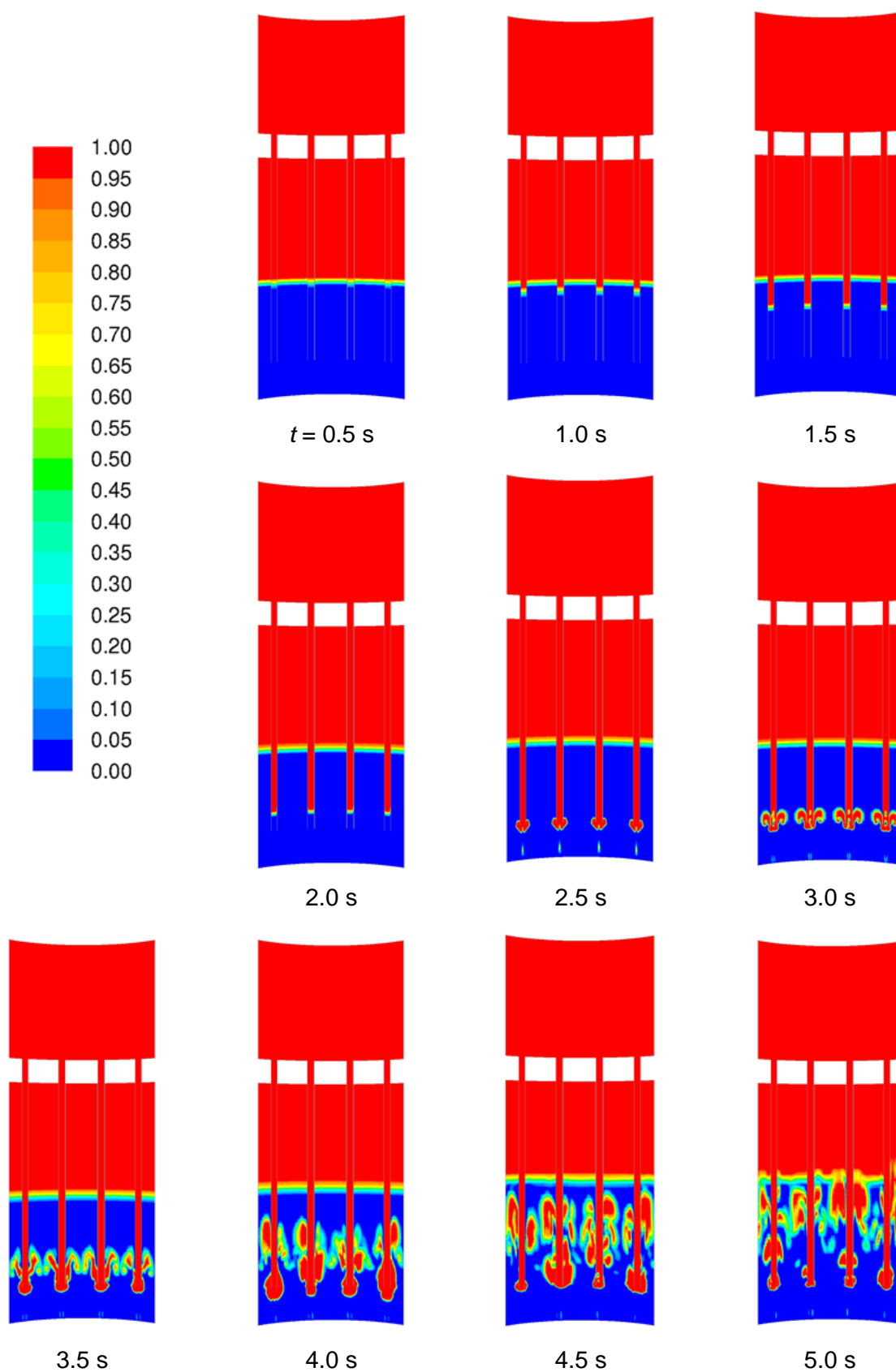


Figure 35. Void fraction on the cylindrical surface that contains axes of the vent pipes (continues on the following page).

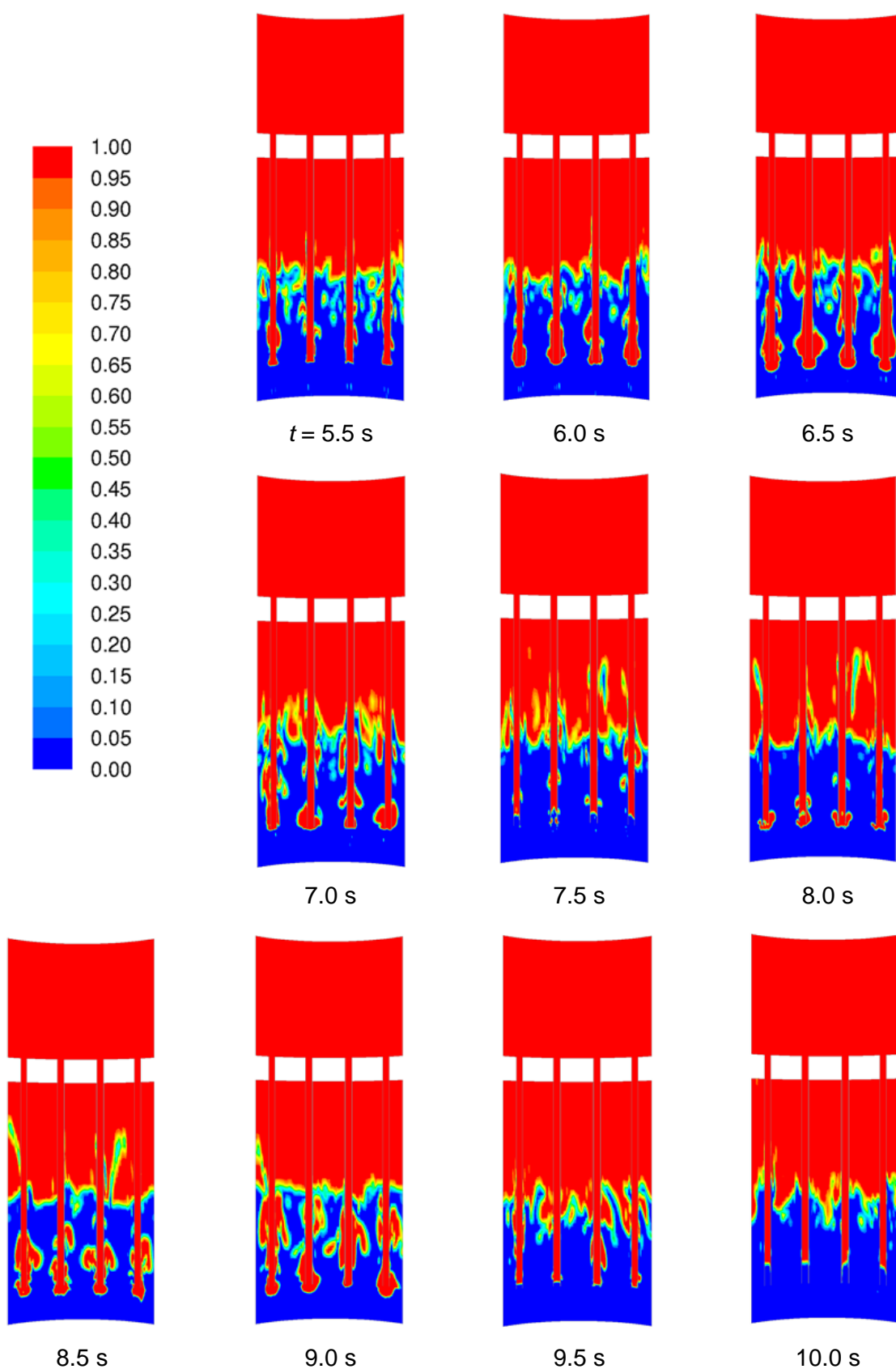


Figure 35. Continues from the previous page.

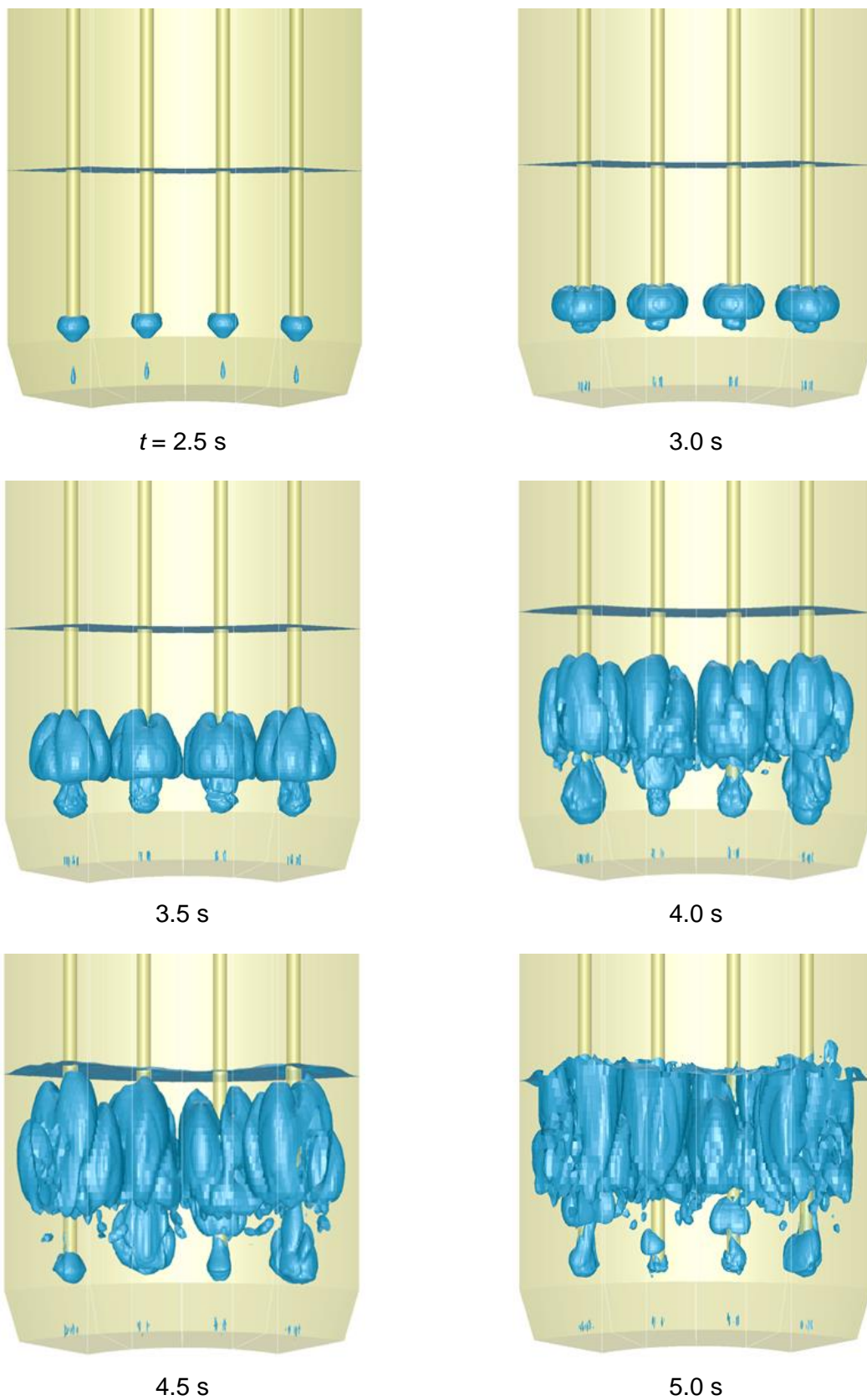


Figure 36. The formation of the first gas bubble in the pressure suppression pool. Iso-surface of void fraction $\alpha = 0.2$ is shown.

In Fig. 37, the time evolution of the absolute pressure is shown. Initially, the pressure in the dry well and in the gas space of the wet well is 100 kPa. At time $t = 2.2$ s, the pressure in the dry well and in the vent pipes has increased by about 71 kPa. This is more than the hydrostatic pressure at the submergence depth of the vent pipes, which is about 67 kPa. The clearance of the vent pipes occurs at this time.

The first gas bubbles breaks the water surface at time $t = 4.8$ s, which is followed by collapse of the water level in the wet well. This incident is followed by pressure oscillation in the wet well around time $t = 5$ s. Some strong pressure oscillations occur in the time interval $t = 8 \dots 10$ s. In particular at time $t = 9.5$ s, the high pressure in the wet well pushes some water back into the vent pipes.

In Fig. 38, the flow velocity of the mixture of the phases is shown. Note that the velocity scale is logarithmic. After the clearance of the vent pipes, the flow velocity in the pipes increases rapidly from 8 m/s to about 50...60 m/s at time $t = 3.0$ s. The flow velocities in the vent pipes do not behave in a fully synchronous manner. Instead, the velocities in the vent pipes are often quite different after time $t = 4.0$ s.

The flow in the vent pipes almost stops or even reverses for a while at a few instants of time. The slowing down or even stopping of the gas flow occurs, when water penetrates into the vent pipes at $t = 5.5$ s, 7.5 and 10 s. Reversal of the direction of the gas flow occurs at time $t = 10$ s in one of the vent pipes. In the second pipe from left, the flow velocity in top part of the pipe is about 0.3...0.4 m/s upwards.

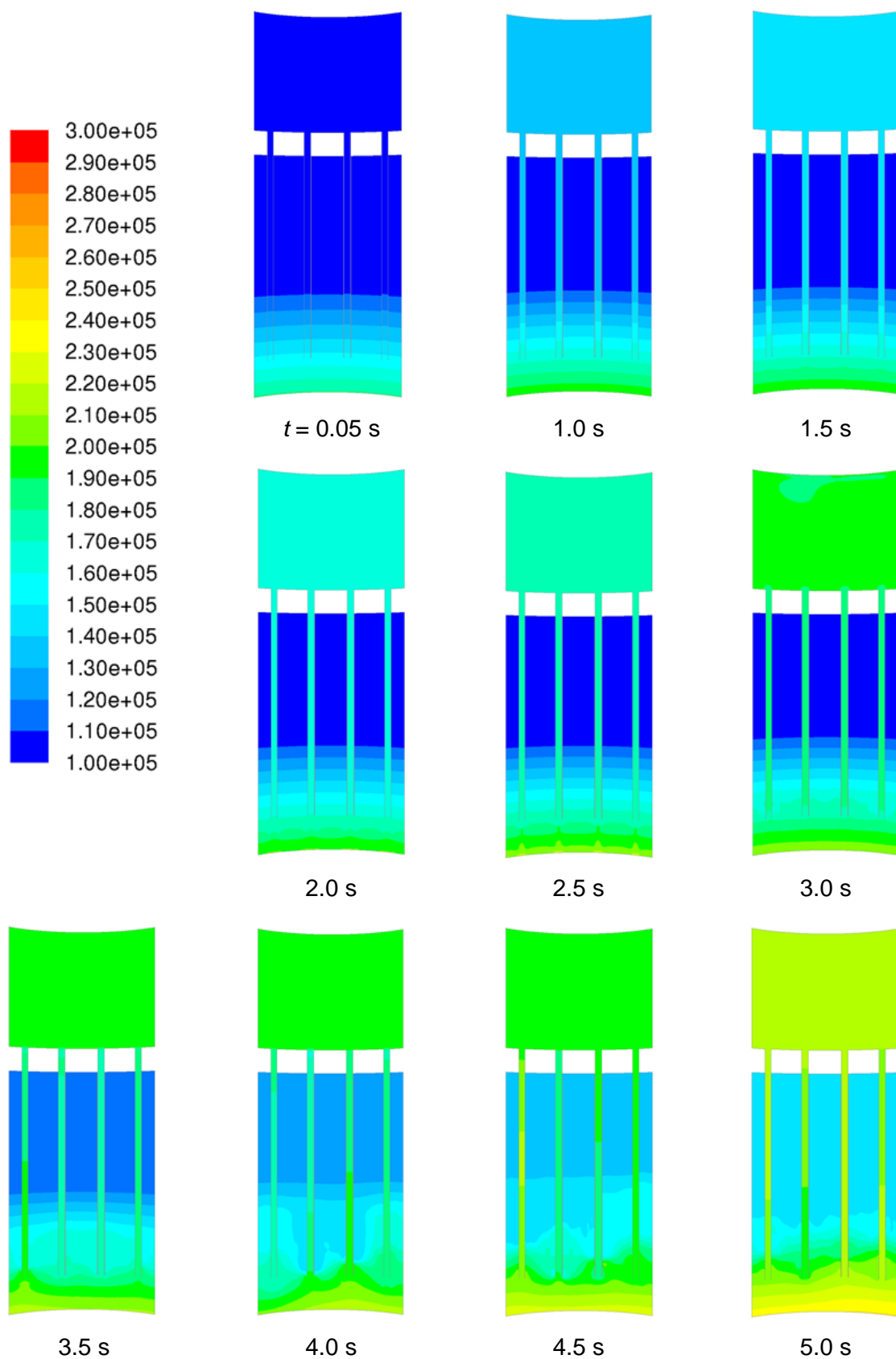


Figure 37. Absolute pressure (Pa) on the cylindrical surface that contains axes of the vent pipes (continues on the following page).

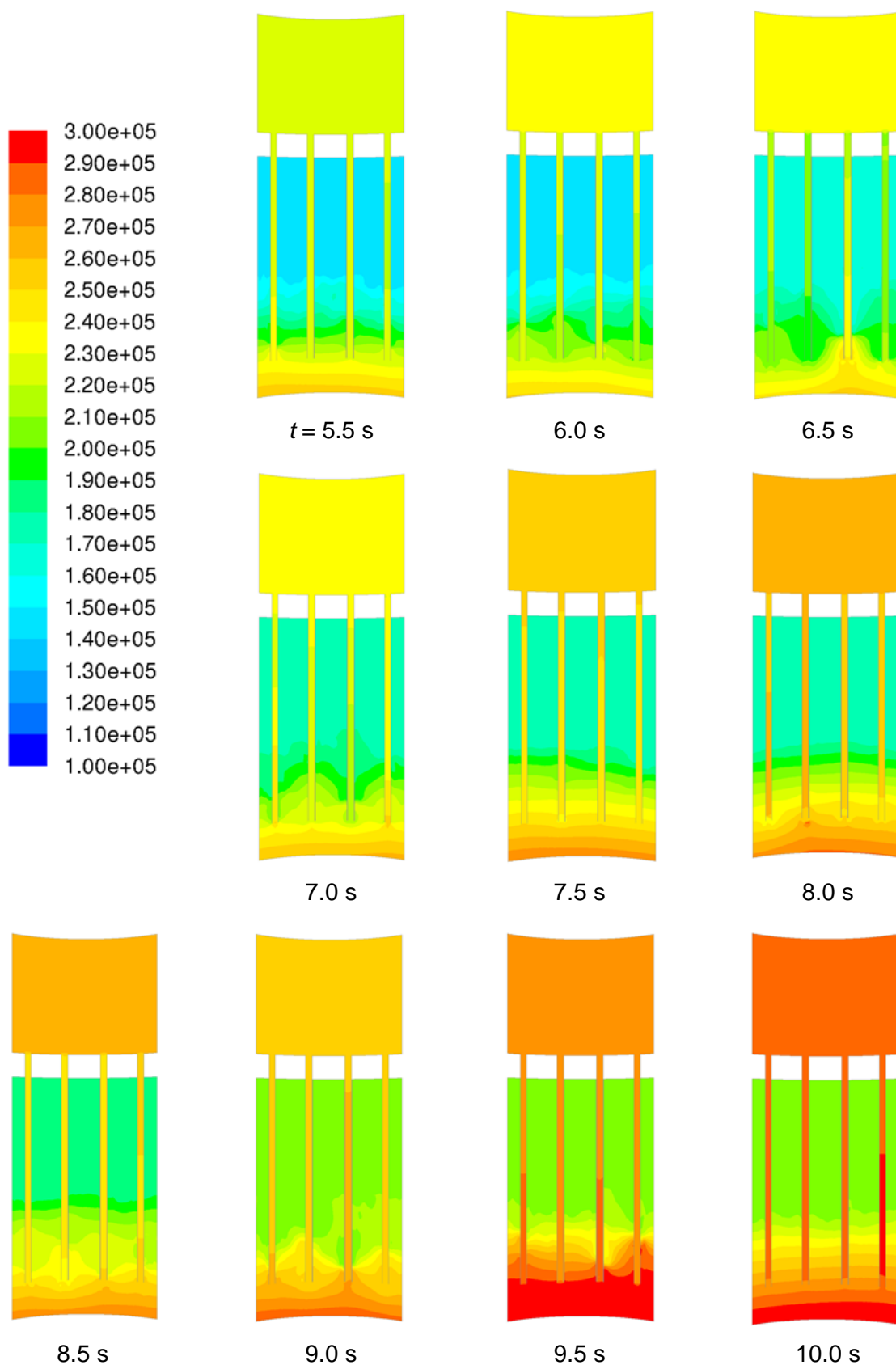


Figure 37. Continues from the previous page.

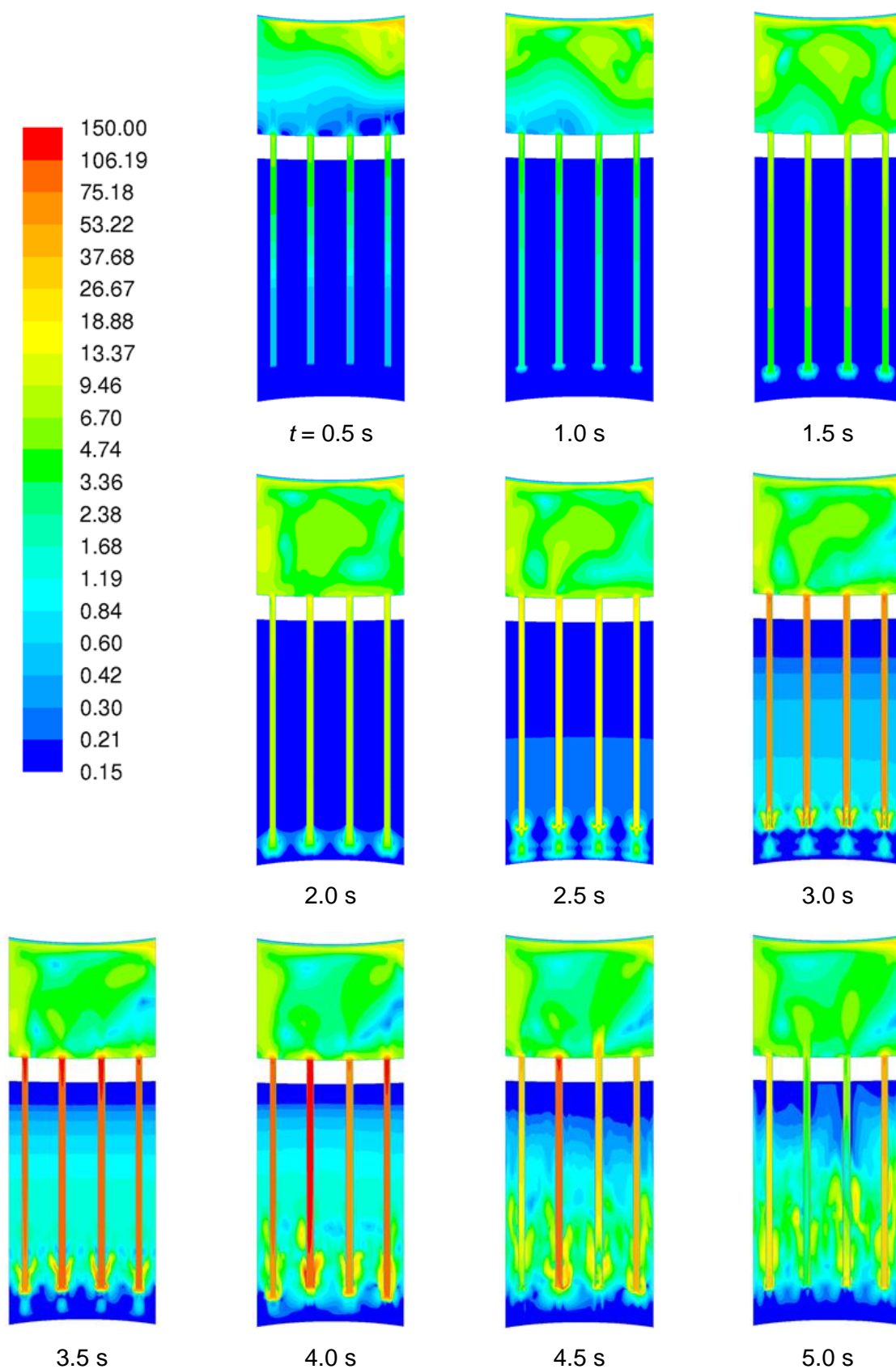


Figure 38. Magnitude of the flow velocity of the mixture of phases (m/s) on the cylindrical surface that contains axes of the vent pipes. Note that the velocity scale is logarithmic (continues on the following page).

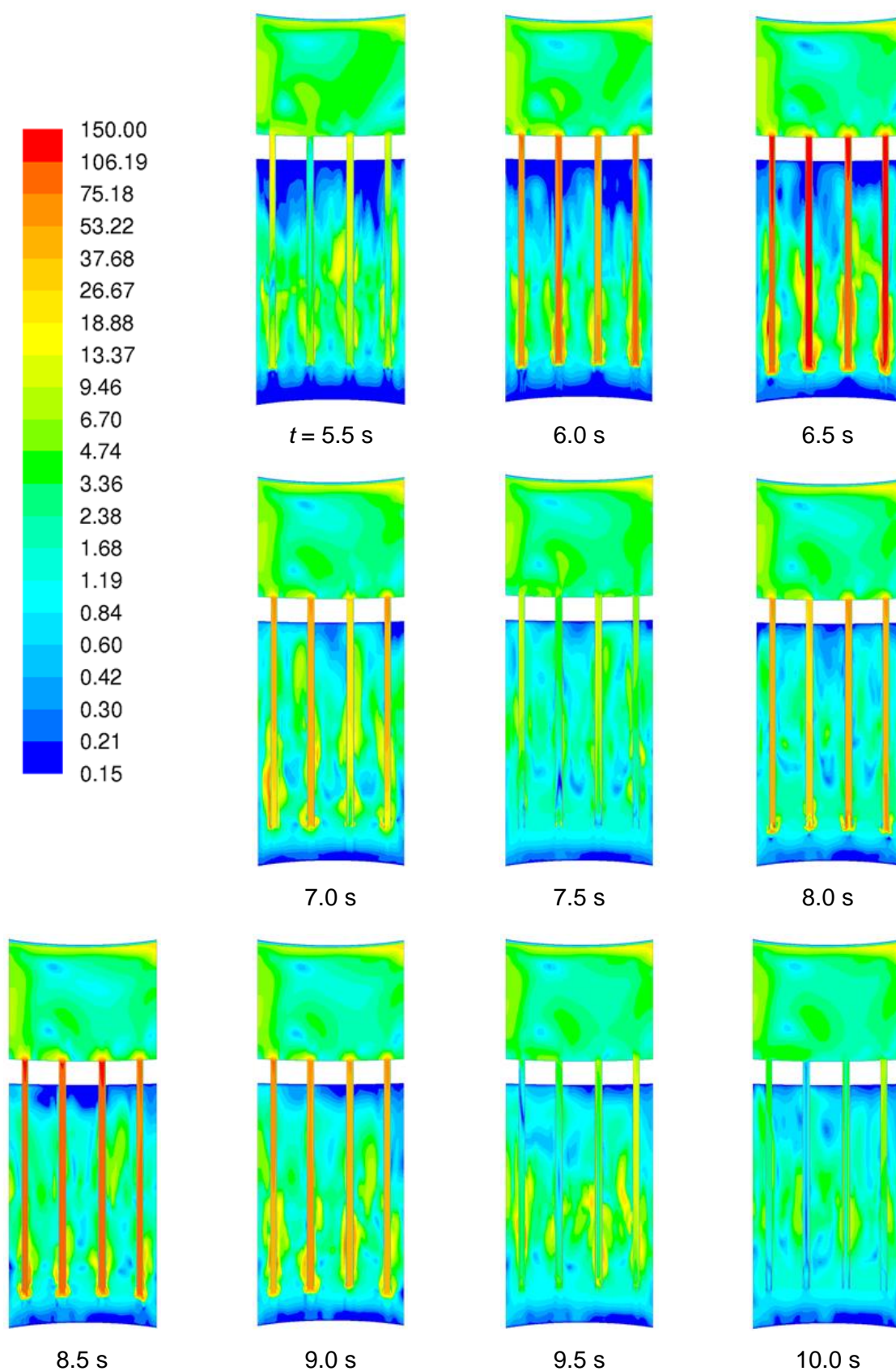


Figure 38. Continues from the previous page.

5. Summary and conclusions

The Computational Fluid Dynamics (CFD) and Finite Element Methods (FEM) used for modelling pressure suppression pool during a postulated Large-Break Loss-Of-Coolant-Accident (LB-LOCA) have been studied. The CFD methods used for the simulation of the early stage of the LB-LOCA have been described and applied to a sector model of a BWR. Fluid-Structure Interaction (FSI) calculations have been performed for the PPOOLEX test facility and a sector model of a BWR. Acoustic FEM method has been applied to a model of BWR containment. In the following, some of the earlier work and results of this report are summarized and conclusions are presented.

CFD methods have been developed by using different approaches. In the early stage of LB-LOCA, blowdown of non-condensable gas has been modeled with the Volume Of Fluid (VOF) method of ANSYS Fluent (Pättikangas et al., 2008). This method has been found to be suitable for modeling the clearance of the vent pipes and it has been found to produce results fairly close to the experimental results obtained with the PPOOLEX facility. The first bubbles of non-condensable gas have also been found to behave similarly to the experiments.

After the early stage of LB-LOCA, different condensation phenomena become important. First, the bulk condensation and wall condensation in the dry well and vent pipes has to be modeled. The modeling of the wall condensation has been performed with the Euler-Euler model of ANSYS Fluent, where models for condensation of steam in air-steam mixture have been implemented. The models have been validated against PPOOLEX experiments (Pättikangas et al., 2009; Pättikangas et al., 2010). The calculated overall amount of condensation on different walls was found to be close to the experimental values, but some differences were also found on different walls.

At later stage of LB-LOCA, the dry well contains only pure steam, which is blown through the vent pipes into the water pool of the wet well. The direct-contact condensation of the steam has been modeled with the Euler-Euler model of ANSYS Fluent, where the condensation models have been implemented (Pättikangas et al., 2011; Timperi et al., 2012). The model for the condensation of pure steam is based on partial pressure approach instead of the diffusion approach used for air-steam mixture. During blowdown of pure steam into the pressure suppression pool, chugging may occur. The Euler-Euler model does not provide sharp interface for large bubbles, but instead a fairly diffuse interface between the phases is obtained. Quantitatively satisfactory results were not obtained for chugging by using this approach.

Laviéville (2008) and Coste (2013) have presented so-called Large Interface model, which is a hybrid model containing features of VOF and Euler-Euler models. Somewhat similar approaches are also being tested by other research groups. The main features of the Large Interface model were implemented in ANSYS Fluent by using User-Defined Functions (Timperi et al., 2014). The implemented model is not currently stable enough for practical calculations in nuclear reactor safety. Therefore, the VOF model or the Euler-Euler model has to be used instead.

In the present work, the early stage of LB-LOCA was calculated by using the VOF model for a 90° sector model of a BWR containing four vent pipes. The CFD model had 2.8 million grid cells, which shows that also full BWR pressure suppression pool can be calculated. For the full size BWR containment, public validation data does not exist. Therefore, the validation of the VOF calculations only relies on the PPOOLEX experiments.

FSI calculations of PPOOLEX experiments and BWR containment have been performed by using several different approaches. First, Star-CD code was coupled with Abaqus FEM code

by using the MpCCI middleware (Pättikangas et al., 2009). Later, direct coupling of Star-CCM+ and Abaqus without any middleware became available. In the present work, this new coupling method has been tested and compared to previously used approaches.

FSI calculations using explicit and implicit two-way coupling of Star-CCM+ and Abaqus codes have been performed. The performance of Star-CCM+ for modelling a propagating pressure pulse in water has first been tested. Numerical damping of the pulse amplitude was considerable with first order time discretization, requiring very short time steps for accurate simulation. With shortest time steps, a double-precision computing accuracy was required. A second order time discretization preserved the pulse amplitude well, but resulted in oscillatory solution. Both the explicit and implicit FSI simulations agreed well with acoustic-structural FEM solutions in a simple piston problem. The implicit simulations enabled the use of fairly large time steps, even when the ratio of structure density to fluid density was decreased such that the explicit solution became severely unstable.

In FSI simulations of the PPOOLEX facility, test calculations with incompressible water were unstable also with implicit coupling while finding a proper under-relaxation factor was required with compressible water. Time and spatial accuracy of the CFD model was found important in modelling the pool loading during the air discharge. Simulations of the early non-condensable phase for a realistic BWR containment showed stable calculations also with explicit coupling when compressible water was assumed. The effect of FSI was small in the BWR containment for the early phase probably due to small displacements and relatively low load frequency.

When chugging occurs during blowdown of steam into the pressure suppression pool, the different vent pipes do not operate fully synchronously. The steam bubbles at different vent pipes collapse at slightly different instants of time. The statistical behavior the chugging has been studied from PPOOLEX experiments and from data published in literature (Timperi et al., 2013, Timperi et al., 2014). The stochastic behavior of 16 vent pipes of a BWR has been studied with the acoustic model of the Abaqus FEM code.

In the present work, the BWR containment FEM simulations have been developed further with different stochastic load applications. The stochastic model for chugging has been used for creating 16 load input files, which have been included into the main Abaqus BWR model input file. The loadings from the vent pipes vary in several ways: the chug events can be desynchronized and the load amplitude and load period can be determined stochastically with the given mean values and standard deviations. Furthermore, any load shape can be applied.

Three different stochastic chugging loading cases were considered. First, chugging events were desynchronized and the load amplitudes were also determined statistically. The standard deviation of the load amplitude was derived from JAERI experiments presented by Kukita and Namatame (1985). Significant differences in the results compared to previous study (Timperi et al., 2014) were not observed. Two sonic velocities were considered: 450 m/s and 1412 m/s. Second, the load period due to chugging and desynchronization between chug events were randomized. Third, the load amplitude was also randomized. The used standard deviation values are only approximate especially for the load period length and a coarse parametric study was performed here. However, the developed methods enable to apply more realistic stochastic loadings if more accurate input statistics are obtained in future.

References

- Abaqus, 2005. Introduction to fluid-structure interaction simulation using Abaqus and Fluent. 2005 Abaqus users' conference, Stockholm, Sweden. Abaqus Inc.
- Björndahl, O. and Andersson, M., 1998. Globala vibrationer vid kondensationsförlopp i wetwell orsakade av LOCA i BWR-anläggningar. Swedish Nuclear Power Inspectorate, SKI Report 99:3, Stockholm, 81 p.
- Causin, P., Gerbeau, J.-F. and Nobile, F., 2004. Added-mass effect in the design of partitioned algorithms for fluid-structure problems. ICES report 04-02, The Institute for Computational Engineering and Sciences.
- Coste, P., 2013. A Large interface model for two-phase CFD, Nuclear Engineering and Design, vol. 255, pp. 38–50.
- Coste P, Pouvreau, J., Laviéville, J. and Boucker, M., 2008. A two-phase CFD Approach to the PTS Problem Evaluated on COSI Experiment, ICONE 16, Orlando, USA, May 11–15.
- Kukita, Y. and Namatame, K., 1985. The vent-to-vent desynchronization effects on LOCA steam condensation loads in BWR pressure suppression pool. Nuclear Engineering and Design 85, pp. 141-150.
- Lahey, R.T., Jr. and Moody, F.J., 1993. The thermal-hydraulics of a boiling water nuclear reactor, 2nd edition, American Nuclear Society, USA.
- Laine, J. and Puustinen, M., 2008. Steam line rupture experiments with the PPOOLEX test facility. Research Report CONDEX 2/2007, Lappeenranta University of Technology, Nuclear Safety Research Unit.
- Laviéville, J. and Coste, P., 2008. Numerical modelling of liquid-gas stratified flows using two-phase Eulerian approach, Proc. 5th Symposium on Finite Volumes for Complex Applications, Aussois, France, June 8-13.
- Moody, F.J., 1990. Introduction to unsteady thermofluid mechanics, Wiley, New York.
- Puustinen, M., Räsänen, A., Laine, J., Purhonen, H., Pättikangas, T. and Timperi, A. 2009. Condensation pool experiments at LUT supporting CFD and structural analysis tool development. 20th International Conference on Structural Mechanics in Reactor Technology, Espoo, Finland, August 9 - 14, 2009.
- Pättikangas, T., Timperi, A., Niemi, J. and Kuutti, J., 2008. Modelling of blowdown of air in the pressurized PPOOLEX facility, VTT Technical Research Centre of Finland, Research Report VTT-R-02233-08, Espoo, Finland, 85 p.
- Pättikangas, T., Niemi, J. and Timperi, A., 2009. Modelling of blowdown of steam in the pressurized PPOOLEX facility. VTT Technical Research Centre of Finland, Research Report VTT-R-03073-09, Espoo, Finland, 52 p.
- Pättikangas, T., Niemi, J. and Timperi, A., 2010a. CFD and FEM modelling of PPOOLEX experiments. VTT Technical Research Centre of Finland, Research Report VTT-R-02187-10, Espoo, Finland, 39 p.
- Pättikangas, T., Niemi, J., Laine, J., Puustinen, M. and Purhonen, H., CFD modelling of condensation of vapour in the pressurized PPOOLEX facility, CFD4NRS-3, 14–16 September 2010, Washington D.C., USA, 12 p.

- Pättikangas, T., Niemi, J. and Timperi, A., 2011. Numerical modelling of pressure suppression pools with CFD and FEM codes. VTT Technical Research Centre of Finland, Research Report VTT-R-00927-11, Espoo, Finland, 53 p.
- Regulatory Guide 1.61, 2007. Damping values for seismic design of nuclear power plants. U.S. Nuclear Regulatory Commission.
- Sigrist, J.F. and Abouri, D., 2006. Numerical simulation of a non-linear coupled fluid-structure problem with implicit and explicit coupling procedures. ASME 2006 Pressure Vessels and Piping Conference, PVP2006-ICPVT-11-93107.
- Sonin, A.A., 1981. Scaling laws for small-scale modelling of steam relief into water pools. Nuclear Engineering and Design, Vol. 65, pp. 17–21.
- Timperi, A., Pättikangas, T., Niemi, J. and Ilvonen, M., 2006. Fluid-structure interaction analysis of a water pool under loading caused by steam injection, VTT Industrial Systems, Research Report TUO72-056662, Espoo, Finland, 64 p.
- Timperi, A. 2009. Fluid-structure interaction calculations using a linear perturbation method. 20th International Conference on Structural Mechanics in Reactor Technology, Espoo, Finland, August 9 - 14, 2009.
- Timperi, A., Chauhan, M., Pättikangas, T. and Niemi, J., 2013. Modelling of pressure loads in a pressure suppression pool. VTT Technical Research Centre of Finland, Research Report VTT-R-01563-13, Espoo, Finland, 54 p.
- Timperi, A., Pättikangas, T. and Niemi, J., 2014. CFD and FEM simulations of pressure suppression pool behaviour. VTT Technical Research Centre of Finland, Research Report VTT-R-00780-14, Espoo, Finland, 54 p.

Title	CFD and FEM modeling of blowdown of gas into pressure suppression pool
Author(s)	Timo Pättikangas, Antti Timperi and Qais Saifi
Affiliation(s)	VTT Technical Research Centre of Finland
ISBN	978-87-7893-420-8
Date	May 2015
Project	NKS-R / ENPOOL
No. of pages	49
No. of tables	2
No. of illustrations	38
No. of references	23
Abstract max. 2000 characters	<p>Computational Fluid Dynamics (CFD) and Finite Element Methods (FEM) used for modelling pressure suppression pool during a postulated Large-Break Loss-Of-Coolant-Accident (LB-LOCA) are summarized. The CFD methods used for the simulation of the early stage of the LB-LOCA are applied to a sector model of a BWR. Fluid-Structure Interaction (FSI) calculations are performed for the PPOOLEX test facility and a sector model of BWR. Acoustic FEM method is applied to a model of BWR containment.</p> <p>FSI calculations using explicit and implicit two-way coupling of Star-CCM+ and Abaqus codes are performed. The implicit simulations enabled the use of fairly large time steps, even when the ratio of structure density to fluid density was decreased such that the explicit solution became severely unstable. Simulations of the early non-condensable phase for a realistic BWR containment showed stable calculations also with explicit coupling when compressible water was assumed.</p> <p>Simulations of a boiling water reactor (BWR) containment with an acoustic FSI FEM model were performed. The BWR containment with 16 vent pipes was loaded stochastically through the pipes. Different statistical cases were considered for applying the loads. A normal distribution curve with the mean value and standard deviation was developed for each varied parameter. The results from different statistical cases were compared.</p> <p>The CFD model for Large Interfaces in two-phase calculations is reviewed and the use of the model for large gas bubbles in pressure suppression pool is discussed. The early stage of LB-LOCA is calculated with a 90° sector model of BWR containment.</p>
Key words	Condensation pool, pressure suppression pool, BWR, CFD, fluid-structure interaction, FSI, chugging, LOCA